Quaternary Science Reviews
December 2015, Volume 129 Pages 111-127
https://doi.org/10.1016/j.quascirev.2015.10.013
https://archimer.ifremer.fr/doc/00294/40516/

North Atlantic Holocene climate evolution recorded by high-resolution terrestrial and marine biomarker records

Moossen Heiko [1, *], Bendle James [1], Seki Osamu [2], Quillmann Ursula [3], Kawamura Kimitaka [2]

[1] Univ Birmingham, Sch Geog Earth & Environm Sci, Birmingham B15 2TT, W Midlands, England.
[2] Hokkaido Univ, Inst Low Temp Sci, Kita Ku, Sapporo, Hokkaido 0600819, Japan.
[3] Univ Colorado, Inst Arctic & Alpine Res, Boulder, CO 80309 USA.

* Corresponding author : Heiko Moossen, email email address : h.moossen@bham.ac.uk

Abstract :

Holocene climatic change is driven by a plethora of forcing mechanisms acting on different time scales, including: insolation, internal ocean (e.g. Atlantic Meridional Overturning Circulation; AMOC) and atmospheric (e.g. North Atlantic Oscillation; NAO) variability. However, it is unclear how these driving mechanisms interact with each other. Here we present five, biomarker based, paleoclimate records (air-, sea surface temperature and precipitation), from a fjordic sediment core, revealing North Atlantic terrestrial and marine climate in unprecedented detail. The Early Holocene (10.7–7.8 kyrs BP) is characterised by relatively high air temperatures while SSTs are dampened by melt water events, and relatively low precipitation. The Middle Holocene (7.8–3.2 kyrs BP) is characterised by peak SSTs, declining air temperatures and high precipitation. A pronounced marine thermal maximum occurs between ~7–5.5 kyrs BP, 3000 years after the terrestrial thermal maximum, driven by melt water cessation and an accelerating AMOC. The neoglacial cooling, between 5.8 and 3.2 kyrs BP leads into the late Holocene. We demonstrate that an observed modern link between Icelandic precipitation variability during different NAO phases, may have existed from ~7.5 kyrs BP. A simultaneous decoupling of both air, and sea surface temperature records from declining insolation at ~3.2 kyrs BP may indicate a threshold, after which internal feedback mechanisms, namely the NAO evolved to be the primary drivers of Icelandic climate on centennial time-scales.

Highlights

► We present five new high-resolution terrestrial and marine biomarker records. ► The multi-proxy approach shows strengths and weaknesses of individual proxies. ► Proxy records reveal leads, lags and drivers of Holocene climate in great detail. ► NAO-type fluctuations govern Icelandic precipitation over most of the Holocene.

Keywords : Iceland, GDGT, Alkenone, n-alkane, Holocene, Climate reconstruction

1. Introduction

A multitude of paleoclimate reconstructions show that the climate of the Holocene, the last ~11.5 kyrs (kilo years), has been far from stable (Bond et al., 2001; Mayewski et al., 2004; Wanner et al., 2011). Prominent climate events include the Holocene thermal maximum (HTM; Kaufman et al., 2004), the 8.2 event (Alley and Ágústsdóttir, 2005), the neoglacial period (Jennings et al., 2002), the Medieval Climate Anomaly (MCA; Graham et al., 2011) and the Little Ice Age (LIA; Ogilvie and Jonsson, 2001). The latter climate events have had significant impacts on human societies (Buntgen et al., 2011; D'Andrea et al., 2011; deMenocal, 2001).

Holocene climatic change is attributed to a plethora of climatic drivers acting on different time scales (Mayewski et al., 2004; Wanner et al., 2011). The overarching external climate driver throughout the Holocene is the changing geometry of Earth's orbit around the sun, which over the last ~ 11 kyrs has driven decreasing summer insolation in the northern hemisphere (Laskar et al., 2004). This orbital cycle affects the climate on millennial and longer time scales by, for example, driving latitudinal shifts of the polar front and the Intertropical Convergence Zone (ITCZ; Haug et al., 2001; Knudsen et al., 2011). Superimposed on this lower-frequency orbital climate driver, higher-frequency volcanic activity and changes in the sun's intensity influence climate on annual to millennial timescales (Gray et al., 2010; Wanner et al., 2011). For example, the Maunder (solar) minimum contributed to the cooler climate of the LIA (Shindell et al., 2001), and recent models link solar activity with climate phenomena such as the North Atlantic Oscillation (Ineson et al., 2011).

The North Atlantic Oscillation (NAO) is the main driver of temperature and precipitation variability in the North Atlantic and Europe (Hurrell, 1995; Hurrell et al.,

79 2003). The NAO describes the strength and directional changes of the westerlies
80 traversing the North Atlantic (Hurrell, 1995). When the NAO is in positive mode (NAO+),
81 westerlies bring moist and warm air masses to Northern Europe (Fig. 1c), while
82 southerly trending westerlies drive a drier and colder climate in Northern Europe when
83 the NAO is in negative mode (NAO-; Hurrell et al., 2003; Fig. 1d). Contemporary
84 observations indicate that the NAO operates over annual to decadal time scales
85 (Hurrell, 1995; Hurrell et al., 2003). However, recent paleoclimate reconstructions show
86 that atmospheric variations, attributed to NAO-type variability, have operated on
87 centennial and even millennial time scales (Olsen et al., 2012; Trouet et al., 2009; Figs.
88 6h, i), contributing to prominent climatic events such as the MCA and the LIA (Trouet et
89 al., 2009). Shifting NAO phases also influence the relative strength of the Irminger and
90 North Icelandic Irminger Currents (IC and NIIC) in the Denmark Strait (Blindheim and
91 Malmberg, 2005), whereby more warm, saline Atlantic Water flows through the
92 Denmark Strait during NAO+, compared to NAO- phases (Figs. 1e, f).

93 The IC and NIIC are part of a network of currents contributing to the Atlantic
94 Meridional Overturning Circulation (AMOC; Hansen and Østerhus, 2000; Vage et al.,
95 2011). The AMOC mediates a significant amount of the pole-ward energy transfer in the
96 northern Hemisphere and contributes to the current mild Northern European climate
97 (Broecker, 1997). Changes in the intensity of the AMOC have been linked to changes in
98 deep water production as indicated by velocity variations of Iceland Scotland Overflow
99 Waters (Hall et al., 2004; Fig. 6k).

100 The solar, atmospheric and oceanic forcing mechanisms described above are
101 some of the drivers that have been invoked to explain the climate evolution of the
102 Holocene (Bond et al., 2001; Harrison et al., 1992; Mayewski et al., 2004). However, the

interactions of these climatic drivers, their relative importance, and the time scales on which they operate are still not well understood. This knowledge gap is evident when considering Bond cycles, which were first described nearly two decades ago (Bond et al., 1997; Fig. 6g). Bond cycles are defined as cyclical (~ 1500 ± 500 years) penetrations of cold surface water, accompanied by drift ice, into the southeast North Atlantic (Bond et al., 1997). Such cycles are thought to be, at least in part, driven by changes in the sun's intensity (Bond et al., 2001). However, other driving mechanisms such as changes in the intensity of the AMOC, changing meridional atmospheric circulation, enhanced regional upwelling, changes in polar water fluxes and NAO indices have also been invoked as possible drivers of Bond cycles (Wanner et al., 2011; and references therein). Despite the number of driving mechanisms that are thought to cause Bond cycles, evidence of these events is not observed in all northern hemisphere paleoclimate records, and many paleoclimate records only show some, and not all of the Bond cycles (Wanner et al., 2011). For example, North Icelandic Shelf diatom and alkenone based sea surface temperature (SST) reconstructions do not show Bond cycles (Bendle and Rosell-Melé, 2007; Justwan et al., 2008; Fig. 6j), even though one might expect distinct N. Atlantic cold SST episodes to be recorded in Holocene sediments from the Icelandic margin.

Iceland and its surrounding waters have received significant scientific attention because climatic archives found in the area integrate proxy responses to most, if not all, climatic forcing mechanisms that have affected Holocene climate in the North Atlantic sector (Andrews and Jennings, 2014; Axford et al., 2011; Geirsdottir et al., 2002; Jennings et al., 2011; Quillmann et al., 2010; Quillmann et al., 2012). Consequently we present five new high-resolution paleoclimate records (n = 326; 1 sample/~30 years; Figs. 6a - e) covering the period between ~10.7 and ~0.3 calibrated kilo years before

present (kyrs BP) from a single sediment core (MD99-2266) from Ísafjarðardjúp fjord in the Denmark Strait (Figs. 1a, b). Fjords are conducive to high sedimentation rates (Howe et al., 2010), facilitating high-resolution paleoclimate reconstructions. Moreover, since fjords bridge the land-ocean interface, paleo-environmental records from fjords provide a unique opportunity to study the link between marine and terrestrial climate. Our five new, biomarker based, reconstructions of three key climatic variables (SST, air temperature and precipitation) represent the most diverse array of marine and terrestrial, high-resolution paleoclimate signals extracted from a single marine archive thus far. The fact that all records are derived from a single sediment core allows their direct comparison without the potential bias inherent to different age models.

The multi-proxy approach is being facilitated by an expanding organic biomarker "toolbox" that enables paleoclimatologists to produce increasingly comprehensive climate reconstructions from a variety of climatic archives (Castañeda and Schouten, 2011; Eglinton and Eglinton, 2008). Here we use this approach to address the following question: to what extent and on what time scales have various climate forcing mechanisms influenced Icelandic SST, MAT and precipitation regimes?

2. Materials and Methods

2.1. Core Location and Oceanography

The Calypso piston core MD99-2266 was retrieved from the mouth of Ísafjarðardjúp fjord, Northwest Iceland (66° 13’77’’ N, 23° 15’93’’ W; Figs. 1a, b), from 106 m water depths, during Leg III of the 1999 IMAGES V cruise aboard the R/V *Marion Dusfresne* (Quillmann et al., 2010 and references therein). It has a 10 cm diameter and a length of 3890 cm.

151 Ísafjarðardjúp fjord is the largest fjord of the Vestfirdir Peninsula. It is ~90 km long
152 and 10 to 15 km wide. Together with its tributary fjords, it covers an area of ~1150 km^2
153 and drains ~2300 km^2 (Andrews et al., 2008). The Drangajökull icecap is located in the
154 north eastern highlands of Vestfirdir Peninsula and its melt waters flow into
155 Ísafjarðardjúp fjord and into Jökullfirðir, which is the largest tributary fjord of
156 Ísafjarðardjúp (Andrews et al., 2008).

157 The core site is affected by two surface currents. The IC is the most westerly water
158 current of the North Atlantic that brings warm Atlantic Water into the Nordic Seas.
159 Today, the volume flux of the IC is estimated to be one Sverdrup (1 SV = 10^6 m^3 s^{-1}) and
160 its heat flux (relative to 0 °C) is estimated to be 25 Terra Watts (Hansen and Østerhus,
161 2000). The IC enters the Denmark Strait and divides into two branches. The NIIC
162 branches off towards the east where it flows onto the North Icelandic Shelf. The second
163 branch flows southwest along the Greenland coast, parallel to the East Greenland
164 Current (EGC; Hansen and Østerhus, 2000). The Polar Front (PF) separates the warm
165 and saline waters carried north by the IC from the colder and fresher polar waters which
166 are carried south by the EGC (Jennings et al., 2011). The location of the PF is
167 determined by the relative strengths of these warm and cold water currents (Ólafsdóttir
168 et al., 2010).

169 **2.2. Age model and Sampling Strategy**

170 The age model of MD99-2266 that was previously published by Quillmann et al.
171 (2010) is used here. It consists of 24 ^{14}C-AMS (Accelerated Mass Spectrometry) dated
172 bivalve and benthic foraminifera shells, as well as the Saksunarvatn tephra, which is
173 located at a sediment depth of 3591 cm (Fig. 2). Quillmann *et al*. (2010) omitted 5 ^{14}C-
174 AMS dates because the dates are older than the underlying dated horizons. Three of

175 those dates are in the top 23 cm suggesting that the core top sediments were disturbed
176 (Quillmann et al., 2010). Quillmann et al. (2010) did not apply an ocean reservoir
177 correction. The mean (2σ standard deviation) error associated with the 19 14C-dates
178 that were used for the final age model, and the Saksunarvatn tephra layer, is ± 165
179 calibrated years. Following Moossen et al. (2013), sample ages were calculated
180 assuming linear sedimentation rates (shown in Fig. 2) between each 14C-AMS dated
181 sediment horizons and between the youngest 14C-AMS date and the core top.

182 Depending on the amount of available sediment, a minimum of 1 cm^3 and a
183 maximum of 6 cm^3 of sediment were sampled from each time horizon. Where the piece
184 of sediment representing a sample of a desired time interval was longer than 6 cm, an
185 equal amount of sediment was taken from the beginning, the middle and the end of the
186 sediment package representing one sample (time) interval. A total of 326 sediment
187 samples were collected.

188 **2.3. Sample preparation and analyses**

189 The methods for sample preparation and biomarker analyses are identical to the
190 ones previously described by Moossen et al. (2013). Samples were solvent extracted
191 using dichloromethane/methanol (3:1 v/v). An internal standard consisting of Squalane,
192 2-Nonadecanone, 1-Nonadecanol and Eruic acid was added to each sample. Samples
193 were fractionated using silica gel column chromatography following Bendle et al. (2007).

194 A gas chromatograph (GC; Shimadzu 2010) with a flame ionisation detector (FID)
195 and a Shimadzu OP2010-Plus Mass Spectrometer (MS) interfaced with a Shimadzu
196 2010 GC were used for the quantitative and qualitative analysis of alkenones and *n*-
197 alkanes (Moossen et al., 2013). Compound separation was achieved using one of two
198 identical columns, either a BP1 (SGE Analytical Science) or a TG-1MS (Thermo

199 Scientific) column (60m, diameter: 0.25 mm, film thickness: 0.25 µm; coating: 100 %
200 Dimethyl-polysiloxane). The GC oven was held at 60 °C for two minutes, then the
201 temperature was ramped up to 120 °C at 30 °C min^{-1} and then to 350 °C at 3 °C min^{-1},
202 where the temperature was held for 20 minutes. An injection standard consisting of
203 methyl behenate was co-injected with each sample.

204 The relative tetraether abundances in 299 MD99-2266 sediment samples were
205 analysed using high performance liquid chromatography-atmospheric pressure
206 chemical ionisation-mass spectrometry (HPLC-APCI-MS) at the Organic Geochemistry
207 Unit at the University of Bristol. Tetraether analysis was identical to that previously
208 described in Moossen et al. (2013).

209 The hydrogen isotopic measurements of the C_{29}-*n*-alkane in 133 samples were
210 conducted at the Institute of Low Temperature Science at the Hokkaido University,
211 Japan. The isotopic values are expressed as per mil (‰; Eq. 1; vs. Standard Mean
212 Ocean Water (SMOW).

213 $$\delta(‰)=((R_{sample}-R_{standard})/(R_{standard}))x1000 \quad \text{Eq. 1}$$

214 The hydrogen isotopic signature of the C_{29}-*n*-alkane (δD_{C29}) was analysed using
215 an HP 6890 GC interfaced with a Finnigan MAT Delta Plus XL MS. The Finnigan MAT
216 combustion furnace was held at 1450 °C. The chromatographic separation of the *n*-
217 alkanes was accomplished using a DB5-HT column (Agilent J&W GC Columns; 30 m,
218 0.25 mm diameter; 0.1 µm film thickness). The following GC oven temperature program
219 was used: the temperature was ramped up from 50 to 120 °C at 10 °C min^{-1}, and then
220 to 310 °C at 4 °C min^{-1}, where the temperature was held for 20 minutes. An external
221 standard consisting of an *n*-alkane mix (C_{16} - C_{30}) with a known hydrogen isotopic

composition was injected daily to evaluate the measurement drift of the instrument and ensure analytical precision. The isotopic composition of the C_{29}-*n*-alkane and of the internal standard (Squalane) was calculated relative to the isotopic composition of an injection standard (Methyl Eicosanoate; δD: -226.8 ‰ vs SMOW) that was co-injected with each sample. The δD value of the internal standard squalane is -179.5 ± 4.7 ‰ (the uncertainty describes the 1σ standard deviation (SD) of squalane in 133 samples over the entire time of analyses). 28 samples were analysed in duplicate and 2 in triplicate, and the 1σ SD of the C_{29}-*n*-alkane relative to the injection standard was ± 3.5 ‰. However, as not all samples were analysed in duplicate due to low *n*-alkane concentrations, we use the internal standard squalane that is present in all 299 samples to determine the analytical precision of the measurements.

2.4. Biomarker and statistical analyses

$U^{K'}_{37}$-SSTs (Fig. 6a) were reconstructed from 326 samples using the relative abundance of the C_{37}-alkenones with two ($C_{37:2}$) and three ($C_{37:3}$) double bonds. Relative abundances were converted into $U^{K'}_{37}$-values after Prahl and Wakeham (1987; Eq. 2). The $U^{K'}_{37}$-values were converted to SSTs using the calibration equation published by Conte et al. (2006; Eq. 3).

$$U^{K'}_{37} = C_{37:2}/(C_{37:2} + C_{37:3}) \quad \text{Eq. 2}$$

$$SST = (U^{K'}_{37}-0.0709)/0.0322 \quad \text{(calibration error of 1.1 °C)} \quad \text{Eq. 3}$$

Thirty-four samples were analysed in triplicate and the mean analytical error (1σ SD) associated with the $U^{K'}_{37}$ index is ± 0.01 which translates into a temperature uncertainty of ± 0.44 °C.

The mean air temperatures (MATs) of 299 samples were reconstructed based on the relative abundance of branched glycerol-dialkyl-glycerol-tetraethers (br-GDGTs; Peterse et al., 2012; Weijers et al., 2007b). The cyclisation ratio (CBT, Eq. 4), and the methylation index of branched tetraethers (MBT', Eq. 5; Peterse et al., 2012) are converted to CBT/MBT'-MATs using the calibration equation published by Peterse et al. (2012; Eq. 6).

$$CBT = -\log([Ib + IIb] / [Ia + IIa]) \quad \text{Eq. 4}$$

$$MBT' = ([Ia + Ib + Ic]) / ([Ia + Ib + Ic]+[IIa + IIb + IIc] + [IIIa]) \quad \text{Eq. 5}$$

$$MAT = 0.81 - 5.67 \times CBT + 31.0 \times MBT' \text{ (root mean square error of 5 °C)} \quad \text{Eq. 6}$$

The roman numerals in equations 3 and 4 refer to the relative abundance of the br-GDGT molecules (Fig. S3; SI 2). Nine samples were analysed in triplicate and two in duplicate and the 1σ SD associated with the CBT/MBT'-MAT measurements is ± 0.5 °C.

Soil pH variations were reconstructed using the revised calibration equation published by Peterse et al. (2012; Eq. 7).

$$pH=7.90-1.97 \times CBT \text{ (root mean square error of 0.8 pH units)} \quad \text{Eq. 7}$$

Nine samples were analysed in triplicate and two in duplicate and the 1σ SD associated with the soil pH measurements is ± 0.04 pH units.

Following Moossen et al. (2013), Average chain length (ACL_{25-35}) values from 310 samples were calculated using the concentrations of the most abundant odd-chained *n*-alkanes with 25 to 35 carbon atoms (Eq. 8; Schefuss et al., 2003). While Moossen et al. (2013) used the ACL_{25-35} record to identify 16 samples as outliers (see also Fig. S2; SI

265 2), the $ACL_{25\text{-}35}$ record, without the 16 outliers is published here and interpreted as
266 showing precipitation change (see discussion below).

267 $$ACL_{25\text{-}35}=(\Sigma(X_i \times C_i)_n)/(C_i)_n \quad \text{Eq. 8}$$

268 X_i represents the *n*-alkanes and C_i represents the abundance of the *n*-alkanes. 11
269 samples were analysed in triplicate and the mean 1σ SD associated with the $ACL_{25\text{-}35}$
270 values is ± 0.06.

271 The C_{29}-*n*-alkane was abundant enough for hydrogen isotopic analysis in 133
272 samples. The δD_{C29} values were corrected for the influence of the global ice volume on
273 the hydrogen isotopic composition of meteoric water following Collins et al. (2013) and
274 Niedermeyer et al. (2010) by using the benthic foraminifera oxygen isotope curve
275 published by Waelbroeck et al. (2002; Fig. S1, SI 2). First, the uncorrected δD_{C29} value
276 were converted to $\delta^{18}O$ values using the meteoric water line equation published by
277 Craig (1961). Then the $\delta^{18}O$ value of each sample was corrected for the influence of ice
278 volume using the 3rd order polynomial equation (Fig. S1, SI 2). Finally, the $\delta^{18}O$ values
279 of the samples were converted back into global ice volume corrected δD_{C29} values (Fig.
280 3).

281 REDFIT spectral analyses were conducted using PAST (Hammer et al., 2001; Fig.
282 7). REDFIT spectral analyses can be performed on unevenly spaced time series
283 (Schulz and Mudelsee, 2002). This pre-empts the need for regular interpolation of the
284 time series presented in this paper. An AR(1) red noise model and the 95 % confidence
285 threshold is fitted to each spectral analyses.

3. Results and Discussion

3.1. Paleoclimate proxies

The $U^{K'}_{37}$-SST proxy is based on variations of $C_{37:2}$ and $C_{37:3}$-alkenones produced by certain haptophyte algae (e.g. *Emiliania huxleyi*) as a response to changing SSTs (Brassell et al., 1986). Previous studies have shown that the $U^{K'}_{37}$-index can be used to reconstruct SSTs on the Icelandic Shelf (Bendle and Rosell-Melé, 2007; Sicre et al., 2011). The $U^{K'}_{37}$-SSTs reported here tend to be higher than those reported previously on the North Icelandic Shelf (Bendle and Rosell-Melé, 2007; Sicre et al., 2011; Fig. 7h). Presumably this is due to the more southerly location of the Ísafjarðardjúp fjord with waters dominated by the warm IC and NIIC (Figs. 1e, f). Additionally, $U^{K'}_{37}$-SSTs are likely biased towards summer due to the predominant production of alkenones during summer months at high latitudes, as suggested for the Icelandic Shelf (Bendle and Rosell-Melé, 2007; Sicre et al., 2008b), the Southern Ocean (Sikes et al., 1997; Ternois et al., 1998) and the Gulf of Alaska (Prahl et al., 2010). This is seemingly confirmed by the close match between core top and mean local summer June/July/August (JJA) SST of 9.6 °C at Stykkishólmur from 1867-1985 (Hanna et al., 2006; Fig. 6a). We assume that most of the sedimentary alkenones are produced locally and note that previous work demonstrates that potential mixing of allochthonous with *in situ* produced alkenones does not disturb the $U^{K'}_{37}$-SST relationship significantly on the Icelandic shelf (Bendle and Rosell-Melé, 2004).

Holocene $U^{K'}_{37}$-SSTs fluctuate between 6.6 °C at ~1.1 kyrs BP, and 14.8 °C at ~7.3 kyrs BP. The mean SST throughout the early Holocene is 10 °C. At the transition from the early to the middle Holocene, the amplitude of SST variability increases, and the onset of the middle Holocene sees the highest reconstructed SSTs (14.8 °C at ~7.3

310 kyrs BP). Between ~5.9 and ~3.2 kyrs BP SSTs decrease from 13.5 to 6.7 °C before
311 rising again during the late Holocene. The mean SST during the late Holocene is 8.9 °C,
312 but with significant variability around the mean throughout the last 2000 years of the
313 record.

314 The CBT/MBT'-MAT reconstruction (Fig. 6b) is based on the variable abundances
315 of br-GDGTs synthesised by subdivisions of *Acidobacteria* (Sinninghe Damsté et al.,
316 2011) and other unspecified soil bacteria (Peterse et al., 2012; Weijers et al., 2007b).
317 There is evidence that br-GDGTs are not amenable to aeolian transport (Gao et al.,
318 2012), indicating that paleo proxies based on these compounds likely reflect a proximal
319 Icelandic signal. The CBT/MBT'-MAT proxy is based on the assumption that br-GDGTs
320 are exclusively produced by terrestrial organisms. Recent work suggests that br-GDGTs
321 may have an aquatic source as well (Fietz et al., 2012), although direct evidence of
322 such a source is still missing (Rueda et al., 2013). The CBT/MBT'-MATs in this study
323 are mainly controlled by variations of just one br-GDGT compound. Throughout the
324 Holocene, the relative concentration of br-GDGT IIIa increases from ~ 10 % to ~ 45 %,
325 while the concentration of the other br-GDGTs remains relatively stable through time (SI
326 2; Fig. S4). The relative abundance of br-GDGT IIIa tracks changes of the previously
327 published BIT-index closely (Fig. 4; Moossen et al., 2013). The BIT-index indicates
328 changes in terrestrial soil input (Hopmans et al., 2004), and has been shown to yield
329 reliable soil input results for Ísafjarðardjúp fjord (Moossen et al., 2013). This infers that
330 GDGT IIIa is mainly derived from local Icelandic soils. Furthermore, previous studies
331 have shown that the relative abundance of br-GDGT IIIa does not change significantly
332 when comparing soils/near shore settings with open marine settings (Peterse et al.,
333 2009; Zhu et al., 2011). These findings suggest that the primary climatic signals,
334 CBT/MBT'-MAT, and also soil pH (see below), are preserved and not confounded by

any changes in terrestrial sediment, or marine vs. terrestrial source dynamics of Ísafjarðardjúp fjord and its catchment area.

Reconstructed CBT/MBT'-MATs follow decreasing Holocene summer insolation closely (r^2 = 0.84; Fig. 5). Therefore we hypothesise that the primary control on CBT/MBT'-MAT is summer insolation change in this study. The close match between core top reconstructed temperatures and the mean instrumental summer air temperature (JJA) of 9.3 °C at Stykkishólmur from 1878-2002 (Fig. 6b; Hanna et al., 2004) seemingly supports the hypothesis that the CBT/MBT'-MATs represent summer season, rather than mean annual temperatures. Furthermore, the reconstructed CBT/MBT'-MATs of the most recent ~1.8 kyrs BP are in good agreement with reconstructed August air temperatures based on chironomid assemblages from north Iceland (Axford et al., 2009; Fig. 7). Finally, even though no clear evidence of a seasonal bias of the CBT/MBT'-MAT proxy has been found in soils at mid-latitudes (Weijers et al., 2011), studies conducted in the Skagerrak (58° N; Rueda et al., 2009) and in Arctic lakes (50° - 73°N; Shanahan et al., 2013) suggest that the CBT/MBT'-MAT proxy represents summer, rather than mean annual temperatures at high latitudes. Both, Rueda et al. (2009) and Shanahan et al. (2013) suggest that the bias towards summer season temperatures may be due to the br-GDGT producing soil bacteria being more active in the summer, when the soils are not frozen or snow covered. Since the calibration equation developed by Weijers et al. (2007b), and refined by Peterse et al. (2012) correlates br-GDGT variability with mean annual temperature (and no alternative summer-season CBT/MBT calibration is currently available), we continue to use CBT/MBT'-"MAT" in the text when referring to the br-GDGT air temperature changes, but we interpret the signal as weighted towards the summer, rather than mean annual temperatures.

360 The mean reconstructed Holocene CBT/MBT'-MAT is 11.8 °C. The highest
361 CBT/MBT'-MAT of 16.6 °C is observed at 9.7 kyrs BP, and the lowest CBT/MBT'-MAT
362 of 7.2 °C is observed at 540 yrs BP. The highest CBT/MBT'-MATs throughout the early
363 Holocene are interrupted by a ~5 °C temperature drop between ~9.7 and ~9 kyrs BP.
364 Subsequently MATs continually decrease from 16.5 °C at ~9 kyrs BP to 8.1 °C at ~3 kyr
365 BP. Throughout the late Holocene, MATs fluctuate around a mean summer temperature
366 of 9.5 °C.

367 Three independent qualitative approaches are presented here to estimate
368 changes in precipitation. Firstly, we infer precipitation variability from soil pH changes
369 that are reconstructed based on br-GDGTs variability (Peterse et al., 2012; Weijers et
370 al., 2007b; Fig. 6c). Soil leaching processes result in soil acidification when precipitation
371 is high (Johnson et al., 1998). The absolute soil pH values presented here suggest
372 more alkaline soil types compared the dominant Icelandic soil type, andosol (Arnalds,
373 2008). Peterse et al. (2010) have shown that the br-GDGT proxy overestimates
374 absolute soil pH values when applied to acidic soils, such as andosol (Arnalds, 2008).
375 Therefore, we do not interpret absolute soil pH values, but rather temporal trends that
376 are indicative of relative pH changes, driven by precipitation variability (Fawcett et al.,
377 2011; Weijers et al., 2007a). As discussed previously, the br-GDGT based CBT/MBT'-
378 MAT proxy likely records a summer season, rather than annual signal, possibly due to
379 increased soil bacterial activity during the summer at high latitudes (Rueda et al., 2009;
380 Shanahan et al., 2013). Consequently, it is likely that the br-GDGT based soil pH proxy
381 also records a summer signal.

382 Secondly, we present two independent proxies based on higher plant wax derived
383 *n*-alkanes that respond to precipitation change. *n*-Alkanes comprise part of the

384 protective wax layer that coats leaves (Eglinton et al., 1962). They are transported via
385 aeolian and fluvial mechanisms into marine sediments and preserved over geological
386 time periods (e.g. Eglinton and Eglinton, 2008, and references therein). Due to the
387 proximity of the core location to land we suggest that the majority of the terrigenous
388 material is derived from the catchment area of Ísafjarðardjúp fjord, likely transported
389 during the spring melt following the winter snowfall maxima that is observed in modern
390 Icelandic annual precipitation (Hanna et al., 2004).

391 The temporal variability of dominant (preferentially produced) leaf wax *n*-alkanes
392 ($ACL_{25\text{-}35}$) is controlled by: contributing plant types (e.g. Rommerskirchen et al., 2006b),
393 ambient air temperature (Kawamura et al., 2003; Vogts et al., 2012) and precipitation
394 regime (e.g. Calvo et al., 2004). The $ACL_{25\text{-}35}$ record presented here exhibits shifts of
395 ~0.5 $ACL_{25\text{-}35}$ units at the transition from the early to the middle, and again from the
396 middle to the late, and throughout the late Holocene (Fig. 6d). These shifts are
397 remarkably large and occur over comparatively short time scales. Elsewhere, similar
398 average chain length shifts have been associated with large scale changes from C_3
399 vegetation dominated landscapes to C_4 vegetation dominated landscapes (and vice
400 versa) over glacial/interglacial time scales (Badewien et al., 2015; Calvo et al., 2004;
401 Rommerskirchen et al., 2006a). Pollen studies from lake sediments and peat deposits
402 show dynamic vegetation variability in Iceland throughout the Holocene. Vestfirdir
403 peninsula vegetation was dominated by Cyperaceae (herbs) and Poaceae (grasses)
404 with small amounts of *Salix*, *Juniperus* and *Betula* (birch) throughout the last 10,000
405 kyrs BP (Caseldine et al., 2003). *Betula* pollen first occured between 7.8 and 7 kyrs BP
406 but never increased above 20 % of the total land pollen sum throughout the pollen
407 record (Caseldine et al., 2003). Elsewhere in northern Iceland birch woodland also
408 became more abundant, until ca. 1000 yrs BP, when it declined again following the

409 settlement of Iceland (Hallsdottir, 1995). Trees produce more short chained *n*-alkanes
410 than grasses (Rommerskirchen et al., 2006b; Vogts et al., 2009). Therefore, it is
411 possible that an increase in the amount of *betula* pollen did contribute to the decreasing
412 ACL_{25-35} values between 7.8 and 7 kyrs BP. However, it is unlikely that the advent of the
413 *betula* occurrence alone is responsible for the large shifts in ACL_{25-35} throughout the
414 record. Furthermore, pollen abundances from lake Vatnskotsvatn (northern Iceland) do
415 not show major variations in the relative amounts of different types of plants (trees,
416 grasses, herbs) between 3.2 and 1 kyr BP (Hallsdottir, 1995), during which time we
417 observe large ACL_{25-35} shifts (of an amplitude equivalent to that observed between 7.8
418 and 7 kyrs BP). Therefore, we suggest that changes in vegetation are not the main
419 driver for ACL_{25-35} shifts observed in MD99-2266 (Fig. 6d).

420 CBT/MBT'-MAT and ACL_{25-35} co-vary throughout the late Holocene suggesting
421 that temperature change may have influenced the leaf wax *n*-alkane distribution over
422 the last 3000 yrs BP. However, no clear linear relationship between the CBT/MBT'-MAT
423 and the ACL_{25-35} records is observed for the entire Holocene (r^2 = 0.1; n = 285)
424 suggesting that temperature is not the main driver for changes in the *n*-alkane
425 distribution. While the linear correlation between the ACL_{25-35} and soil pH records (r^2 =
426 0.2; n = 285) is only marginally stronger, the long term co variation of the ACL_{25-35} and
427 the soil pH record suggests that the ACL_{25-35} responds to changes in precipitation.
428 Assuming that leaf waxes are produced during the main growing season of plants at
429 high latitudes, they likely record spring/summer, rather than annual precipitation.

430 The hydrogen isotopic composition of the C_{29}-*n*-alkane (δD_{C29}) is used as an
431 additional proxy for precipitation change (Fig. 6e). The photosynthesis of organic matter
432 by terrestrial higher plants utilizes soil water that ultimately derives from precipitation

433 (Sachse et al., 2012). The hydrogen isotopic compositions of leaf wax derived *n*-alkanes
434 consequently reflect changes in precipitation and are an established proxy to
435 reconstruct paleo-precipitation regimes (Sachse et al., 2012; Schefuss et al., 2005). The
436 spatial and temporal isotopic variability of precipitation is controlled by hydrological
437 variables, the continental, temperature and amount effects, and these need to be
438 considered when interpreting the δD_{C29} isotopic signature (Sachse et al., 2012). For at
439 least the last 1000 years, the amount of precipitation Iceland receives has been driven
440 by the NAO (Hurrell, 1995; Trouet et al., 2009). Iceland receives more precipitation
441 during NAO+, compared to NAO- phases (Hurrell, 1995). The close link between the
442 NAO and precipitation amounts suggests that the main moisture source for Icelandic
443 precipitation is the moisture transported by the westerly storm track that traverses the
444 North Atlantic (Figs. 1c, d). While the latitudinal trajectory and the strength of these
445 westerlies has decreased throughout the Holocene, their direction has remained the
446 same (Harrison et al., 1992), suggesting that the hydrogen isotopic variability observed
447 here cannot be attributed to major changes in water source areas. Therefore, we
448 postulate that the δD_{C29} variability in the studied area reflects shifting NAO modes due
449 to different precipitation regimes at least in the late Holocene. In the early Holocene,
450 relatively high temperatures likely also influenced the isotopic signature of leaf wax
451 components and will be discussed later.

452 The soil pH, ACL_{25-35} and δD_{C29} proxies all show remarkably similar millennial to
453 centennial variability, particularly in the late Holocene (Figs. 6 and 7c, d, e). Therefore,
454 we are confident that the interpretation of all three proxies in concert allows a robust
455 interpretation of relative changes in precipitation.

456 The average proxy values spanning the Holocene are 7.9 for soil pH, 29.12 for
457 $ACL_{25\text{-}35}$, and -197 ‰ for δD_{C29} (Figs. 6c, d, e). The combined precipitation proxy
458 records tend towards less than average precipitation from ~10.7 to 7.8 kyrs BP,
459 increased precipitation from ~7.8 to ~3 kyrs BP and considerable fluctuation around the
460 mean throughout last 3 kyrs BP of the records.

461 **3.2. Comparing terrestrial and marine biomarker records**

462 Magnetic susceptibility data from Ísafjarðardjúp and its tributary fjords shows that
463 the post glacial sedimentation history has been very dynamic (Andrews et al., 2008).
464 For example, high concentrations of magnetic minerals in early Holocene sediments
465 reflect the final deglaciation of Iceland (Andrews et al., 2008). Such a dynamic
466 sedimentation history has also been inferred through changing inputs of terrestrial vs.
467 marine organic matter into Ísafjarðardjúp (Moossen et al., 2013). Moossen et al. (2013)
468 argue that the build-up of soil and plant biomass in the aftermath of deglaciation, and
469 subsequent soil erosion during the Neoglacial, and settlement of Iceland, led to a ~10 %
470 increase in sedimentary terrestrial organic matter content in Ísafjarðardjúp ford from the
471 early, through the middle, into the late Holocene. Dynamic erosion and sedimentation of
472 terrestrial organic matter throughout the late Holocene has also been described in lake
473 Haukadalur (Geirsdottir et al., 2009b), which lies just south of the Vestfirdir Peninsula. It
474 is conceivable, as is the case in lake Haukadalur (Geirsdottir et al., 2009b), and in a
475 Canadian fjord (Smittenberg et al., 2006), that increased sedimentation of terrestrial
476 organic matter in the late Holocene, may have led to the deposition of a mix of fresh and
477 old biomarkers. However, the comparison of the terrestrial biomarker data with other
478 palaeoclimate records (see discussion below) clearly indicates that the biomarkers
479 analysed in this study record climatic events. For example, the CBT/MBT'-MAT proxy
480 follows declining insolation in the early, and middle Holocene. Additionally, when

481 comparing the five biomarker records to palaeo-NAO reconstructions (Olsen et al.,
482 2012; Trouet et al., 2009) the records collectively show a synchronous response (see
483 discussion below). Thus, the palaeoclimate records presented here indicate that the
484 influence of old/reworked organic carbon was not significant enough to confound
485 primary climatic signals.

486 Many of the conclusions drawn from the five biomarker records presented in this
487 paper are based on the assumption that the temporal offset between the production and
488 sedimentation of the different biomarkers does not exceed the resolution of the
489 biomarker records. The integral prerequisite to this assumption is that the time it takes
490 for the studied biomarkers to be transported from their respective precursor organisms
491 into the sediment is similar enough that the interpreted signals indeed reflect the same
492 climate events. Even if lateral transport of a small portion of alkenones is assumed,
493 alkenones still have the most direct transport pathway into marine sediments compared
494 to terrestrially derived br-GDGTs (Gao et al., 2012), that are thought to be mainly
495 transported via fluvial mechanisms, and higher plant wax *n*-alkanes, that are
496 transported via aeolian and fluvial mechanisms (e.g. Eglinton and Eglinton, 2008, and
497 references therein). Here too, the synchronous response of the five biomarker records
498 to NAO variations in the late Holocene suggests that the transport times of different
499 biomarkers to the sediment are at least similar enough to resolve centennial scale
500 climatic changes.

501 **4. Holocene climate evolution**

502 The five combined paleoclimate records from Ísafjarðardjúp fjord reveal terrestrial
503 and marine climate in unprecedented detail for a marine sediment core record covering
504 the entire Holocene (Figs. 6a-e). The combination of proxy records allows the

505 placement of new constraints on the relative importance of different climatic drivers for
506 Icelandic climate throughout the Holocene. Below we discuss how the climate of the
507 early, middle and late Holocene was likely driven by the changing relative influence of
508 large-scale climatic drivers.

509 Concerted inspection of the $U^{K'}_{37}$-SST, the CBT/MBT'-MAT, and the precipitation
510 records highlight two noteworthy and distinct climatic shifts at ~7.8 and ~ 3.2 kyrs BP
511 (Fig. 6). No one individual proxy record clearly delimits these phase shifts, which is
512 expected as individual proxies are recording marine or terrestrial temperatures or
513 precipitation. These climatic parameters inherently have differential responses and
514 sensitivity to external drivers and internal climate forcing mechanisms. Even in the case
515 of the three proxies which record precipitation, different biogeochemical (biosynthesis of
516 lipids) and physical processes (isotopic fractionation) are involved in transcribing the
517 climatic signal, with a varying degrees of fidelity.

518 In the following section we will discuss the competing driving mechanisms that
519 likely drove the climatic shifts at ~7.8 and ~3.2 kyrs BP. We explore the changing
520 relative importance of the climate drivers, as they shaped the three distinct climatic
521 periods of the Holocene.

522 **4.1. Early Holocene and glacial aftermath (10.7 to 7.8 kyrs BP)**

523 The CBT/MBT'-MAT reconstruction indicates that Icelandic terrestrial air
524 temperatures were considerably warmer during the early Holocene than at any other
525 time covered by the record (Fig. 6b). This observation is synchronous with a maxima in
526 high northern hemisphere summer insolation (Laskar et al., 2004). Indeed, it is the close
527 correlation between the reconstructed CBT/MBT'-MATs and summer insolation
528 throughout the early and the middle Holocene, which indicates that summer insolation

529 was the main driver for summer season terrestrial climate (Fig. 5). The CBT/MBT'-MAT
530 record also reveals that the terrestrial Holocene thermal maximum occurred between
531 ~10.5 and ~8.5 kyrs BP. This timing broadly agrees with chironomide based
532 temperature reconstructions, which indicate a terrestrial warm period between ~10.5
533 and 7.5 kyrs BP (Caseldine et al., 2003; Langdon et al., 2010). Increased primary
534 production in lake Hvítárvatn also indicate warm summers between 10.2 and 9 kyrs BP
535 (Larsen et al., 2012). Interestingly, there is no clear 8.2 kyr signal in the climate records
536 presented here, compared to the GISP 2 oxygen isotope record (Grootes and Stuiver,
537 1997; Fig. 6i). The CBT/MBT'-MAT does drop during the period coinciding with the 8.2
538 kyr event, but the decrease is not significant when viewed in context of the early (and
539 entire) Holocene record (Fig. 6b). Our sample resolution (27 samples between 8 - 8.4
540 kyrs BP: 1 sample/~15 yrs BP), is sufficient to capture the 8.2 kyr event, which lasted
541 for *ca.* 400 years (Alley and Ágústsdóttir, 2005). However, there is only one data point
542 within the period of the 8.2 kyr event that shows a noteworthy CBT/MBT'-MAT
543 decrease. This suggests that either a) the 8.2 kyr event did not exert a significant
544 influence on Icelandic terrestrial climate, or b) the CBT/MBT'-MAT proxy does not
545 record it. The latter explanation is most likely, given that, numerous records suggest a
546 significant impact of the 8.2 kyr event on climate in the North Atlantic sector (Alley and
547 Ágústsdóttir, 2005; Quillmann et al., 2012; Rohling and Palike, 2005). Rohling and
548 Palike (2005) find evidence that paleoclimate proxies biased towards summer seasons,
549 do not record the 8.2 kyr event clearly. This is consistent with the CBT/MBT'-MAT proxy
550 that likely records summer, rather than mean annual temperature at high latitudes (see
551 discussion above).

552 $U^{K'}_{37}$-SSTs do not show a clear relationship with insolation during the early
553 Holocene (Fig. 6a). Indeed, while summer insolation peaked throughout the first 700

554 years of the Holocene, Icelandic $U^{K'}_{37}$-SSTs decreased by nearly 1.5 °C from ~10.7 to
555 ~10 kyrs BP, before levelling out at ~9 °C for the next 900 years. $\delta^{18}O$ analyses of
556 foraminifera reveal that the IC started to influence the northern Denmark Strait 11 kyrs
557 BP ago and was fully established by 10.2 kyrs BP (Ólafsdóttir et al., 2010).
558 Reconstructed high marine paleoproductivity in Ísafjarðardjúp fjord during much of the
559 early Holocene also points towards a penetration of nutrient rich Atlantic waters to the
560 core site (Moossen et al., 2013). Despite the relatively warm Atlantic water transport of
561 the IC, the occurrence of sea-ice indicating foraminifera and diatoms suggests that the
562 Denmark Strait was also influenced by glacial melt water pulses, and/or repeated lateral
563 shifts of the polar front (Andersen et al., 2004; Jennings et al., 2011). Benthic
564 foraminiferal $\delta^{18}O$ analyses from Ísafjarðardjúp fjord indicate that the coring site was
565 influenced by glacial melt water throughout the early Holocene (Quillmann et al., 2010).
566 Such melt water pulses can be attributed to a second, regional, climate driving
567 mechanism: the residual melting of northern hemisphere ice sheets following the last
568 glacial maximum. After the glacial advance throughout the Younger Dryas, the main ice
569 sheet covering the Icelandic Highlands was retreating at 10.3 kyr BP (Geirsdottir et al.,
570 2009a), and the distal Greenland (Jennings et al., 2011), and Laurentide ice sheets
571 (Alley and Ágústsdóttir, 2005) were also melting. Continual sea level rise suggests that
572 land locked glaciers melted throughout the early, and into the middle Holocene until ~7
573 kyr BP (Siddall et al., 2010). Therefore, we attribute the dampened $U^{K'}_{37}$-SSTs, that are
574 divergent from the CBT/MBT'-MAT trend and solar insolation, to the pervasive influence
575 of glacial melt water in the early Holocene.

576 The early Holocene $U^{K'}_{37}$-SST record reveals two warm periods wherein SSTs
577 rose by up to 2 °C, lasting from ~8.9 to ~8.5 kyrs BP and from ~8.1 to ~7.9 kyrs BP, that
578 coincide with periods of high sunspot numbers (Solanki et al., 2004; Fig. 6f). Peak to

579 peak comparison of these intervals reveals that cooler background climate between
580 ~8.5 and ~7.9 kyrs BP may have been driven by generally low sunspot numbers, with
581 SST peaks coeval with transient spikes in solar activity. A similarly long (8.7 to 7.9 kyr
582 BP) cool period is also evident from two lacustrine sites in central and north Iceland
583 (Geirsdóttir et al., 2013; Larsen et al., 2012). The link between low sunspot numbers
584 and low $U^{K'}_{37}$-SSTs is supported by Rohling and Palike (2005), who hypothesise that
585 proxies reconstructing summer climate are driven by the suns activity. Modern Icelandic
586 coastal waters feature an insolation induced thermocline during the summer months,
587 resulting in a sharp temperature gradient from warmer surface waters to cooler deeper
588 waters (Hanna et al., 2006). It seems likely that the Ísafjarðardjúp fjord water column
589 was similarly, if not more stratified during the early Holocene when high summer
590 insolation and glacial melt water events occurred. This mechanism could explain the
591 coherence noted above between solar activity and the $U^{K'}_{37}$-SST proxy. We note that
592 there is no discernible relationship between $U^{K'}_{37}$-SSTs and sun spot numbers
593 elsewhere in the early Holocene, possibly due to internal mechanisms, e.g. melt water
594 events causing colder SSTs and masking the effect of increased solar activity on the
595 $U^{K'}_{37}$-SSTs.

596 The hypothesis that $U^{K'}_{37}$-SSTs are likely biased towards summer season
597 temperatures may also explain the lack of a notable $U^{K'}_{37}$-SST drop during the 8.2
598 event, since Rohling and Palike (2005) suggest that summer season proxies do not
599 sensitively record the 8.2 event. In contrast to the $U^{K'}_{37}$-SSTs, the $\delta^{18}O$ record of benthic
600 foraminifera from the same sediment core indicates a cooling and freshening of the IC
601 at this time (Quillmann et al., 2012). Therefore, the biomarker and $\delta^{18}O$ proxy records
602 reveal a possible decoupling of surface photic zone summer temperatures from deeper

603 thermocline temperatures and increased stratification of the Denmark Strait water
604 column during the early Holocene summer season.

605 All three precipitation records indicate that Iceland experienced a dryer than
606 average summer climate during the early Holocene. Models indicate that the Icelandic
607 low was located further north and stronger, than present, driving a stronger westerly jet,
608 with increased precipitation and temperatures in winter (Harrison et al., 1992). The
609 summer simulation of the same model suggests a reduced westerly jet during summer
610 that would have led to a drier summer climate in north and central Europe (Harrison et
611 al., 1992). Our precipitation proxies likely reflect summer, rather than winter precipitation
612 (see discussion above), explaining their agreement with the modelled summer climate
613 of the early Holocene. Not only the strength, but also the more northerly trajectory of the
614 westerlies traversing the North Atlantic (Harrison et al., 1992; Knudsen et al., 2011) may
615 have affected the precipitation regime. The proximity of the Greenland and Laurentide
616 ice sheets may have contributed to the cooling of the westerlies causing them to hold
617 less moisture and consequently resulting in a dryer Icelandic summer climate
618 throughout the early Holocene. Finally, melt water induced cooling of regional SSTs
619 may have contributed to lower precipitation: cold water evaporates less readily than
620 warmer water, yielding relatively dryer maritime air masses, subsequently reduced
621 precipitation on adjacent land masses.

622 The relatively high insolation and air temperatures coupled with the drier climate of
623 the early Holocene would have caused relative increases in soil water evaporation and
624 leaf water transpiration, leaving the available water for *n*-alkane biosynthesis depleted
625 of the light isotope (Sachse et al., 2012). We argue that this depletion is reflected in the

626 high δD_{C29} values measured during the early Holocene, compared to the average
627 Holocene conditions (Fig. 6e).

628 Interestingly, our record indicates that leaf wax isotopic values dropped by nearly
629 10 ‰ at the onset of the 8.2 kyr event and then recovered afterwards. None of the other
630 climate proxies (both temperature and precipitation) show a significant response to the
631 8.2 kyr event. Models suggest the catastrophic influx of glacial melt-waters resulted in
632 isotopically depleted surface waters in the North Atlantic region for decades after the
633 initial event, regardless of the isotopic effects of any synchronous changes in
634 temperature and precipitation (LeGrande and Schmidt, 2008). Thus in our record the
635 transient changes to more negative isotope values at 8.2 kyr BP (and perhaps at 8.7 kyr
636 BP) may reflect changes in the δD of the precipitation source, rather than local climate
637 impacts or a change in precipitation source/pathway.

638 **4.2. Mid-Holocene and Neoglaciation (7.8 - 3.2 ka)**

639 At the transition from the early to the middle Holocene, while summer insolation
640 and CBT/MBT'-MAT decreased, two rapid $U^{K'}_{37}$-SST warming events occurred (Fig. 6a).
641 Centred on 7.6 and 7.3 kyr BP, both events lasted ~300 years, during which $U^{K'}_{37}$-SSTs
642 spiked by ~5 °C (rising by a remarkable 0.5 °C per decade). Following the second event
643 SSTs rose steadily over the next 1400 years by ~4 °C. These $U^{K'}_{37}$-SST peaks coincide
644 with Bond cycles 5 and 4 (Fig. 6g). We term the period between 7.8 and 5.5 kyrs BP the
645 'marine Holocene thermal maximum (HTM)' as the highest $U^{K'}_{37}$-SSTs are observed
646 during this interval. The marine HTM broadly coincides with diatom and coccolithophore
647 based evidence for increased Atlantic water penetration onto the northwest Icelandic
648 Shelf (Giraudeau et al., 2010; Justwan et al., 2008) and the highest SSTs observed off
649 of south east Greenland (Jennings et al., 2011) and the North Icelandic Shelf (Justwan

et al., 2008; Fig. 6j) Furthermore, a major increase in reconstructed flow speed of the North Atlantic deep water across the Iceland-Scotland overflow ridge is centred on 7.2 kyr BP (Hall et al., 2004; Fig. 6k). As regional components of the AMOC, deep-water flow speeds across the Iceland-Scotland ridge and the northward flow of warm surface currents in the Nordic Seas (including the Denmark Strait) are thought to be linked (Hall et al., 2004; Renssen et al., 2005), suggesting increased AMOC velocity acting as a contributing driver for the high $U^{K'}_{37}$-SSTs of the marine HTM.

The cessation of glacial melt water events at the transition from the early to middle Holocene affords a complimentary explanation for the marine HTM. $\delta^{18}O$ signatures of *C. lobatulus* show that melt water pulses stopped affecting Ísafjarðardjúp waters from 7.9 kyr BP onwards (Quillmann et al., 2010). Intriguingly this coincides with the start of the first rapid $U^{K'}_{37}$-SST warming event noted above (Fig. 6a). This suggests that, once the dampening effect of glacial melt-water was removed, the still high (albeit decreasing) solar insolation, combined with a period of increased AMOC flow speed, drove a series of high SST episodes in Ísafjarðardjúp fjord.

The most striking observation when comparing the CBT/MBT'-MAT and $U^{K'}_{37}$-SST records is the temporal offset of ~3000 years between the maxima of the terrestrial HTM (~9.5 kyr BP) and the marine HTM (~6.5 kyr BP). Terrestrial and marine paleoclimate archives in the Iceland/Greenland region indicate that the HTM started at 8.6 ± 1.6 kyrs, and ended at 5.4 ± 1.4 kyrs (Kaufman et al., 2004). The uncertainties associated with the onset and end of the HTM may be due to the time it takes biologically based proxies to adjust to the HTM, i.e. the time it took *Betula* pollen to form mature vegetation and subsequently enough of a sedimentary pollen signature to be found in the paleoclimate record (Caseldine et al., 2003; Kaufman et al., 2004).

674 However, uncertainties in the timing of the HTM may also be due to the delayed
675 response of specific parts of the environment to solar insolation as a climatic driver
676 (Kaufman et al., 2004). One example is the spatial variability of the onset/termination of
677 the HTM across the European/American Arctic sector. While the residual Laurentide ice
678 sheet may have prevented the HTM from being expressed at sites surrounding the
679 Hudson Bay, proxy records from Iceland were already influenced by the HTM (Kaufman
680 et al., 2004).

681 In line with the latter explanation, we attribute the observed temporal discrepancy
682 between the terrestrial and the marine HTM to the different responses of terrestrial and
683 marine environments to solar radiation. Specifically, melt-water pulses dampened $U^{K'}_{37}$-
684 SSTs during the early Holocene while CBT/MBT'-MATs were already driven by high
685 insolation. Subsequently, $U^{K'}_{37}$-SSTs rose rapidly to form the marine HTM, 'delayed' by
686 ~3000 years, but driven by declining, yet still high solar insolation, and possibly an
687 accelerating AMOC.

688 We place the late Holocene neoglaciation between ~5.8 and ~3.2 kyrs BP, where
689 both the $U^{K'}_{37}$-SST, and the CBT/MBT'-MAT records indicate decreasing temperatures
690 in tandem with decreasing summer insolation. This corroborates observations from
691 marine (Jennings et al., 2002; Justwan et al., 2008; Fig. 6j; Moros et al., 2006), and
692 terrestrial records from Iceland (Geirsdóttir et al., 2013; Larsen et al., 2012; Moossen et
693 al., 2013; Wastl et al., 2001). The neoglaciation culminated at ~3.2 kyrs BP with some
694 of the lowest $U^{K'}_{37}$-SST and CBT/MBT'-MAT temperatures observed (Figs. 6a, b),
695 coinciding with a global cool episode recognised in a number of records (Mayewski et
696 al., 2004 and references therein). The late neoglacial decline in marine and terrestrial
697 temperatures is clearly driven by declining insolation. However, an additional driver may

698 have been the decelerating AMOC (contributing to the $U^{K'}_{37}$-SST decrease), culminating
699 in the 2.7 ka event, as evidenced by declining Iceland Scotland overflow velocities (Hall
700 et al., 2004; Fig. 6k).

701 The soil pH and $ACL_{25\text{-}35}$ precipitation proxies (and to a lesser degree the δD_{C29}
702 proxy) show a transition from less than average, to more than average precipitation at
703 the onset of the middle Holocene (Figs. 6c,d,e) through to its termination ~3.2 kyr BP
704 ago. Increasing precipitation throughout the middle Holocene is consistent with
705 increased windiness/storms in Iceland and Greenland (Jackson et al., 2005; O'Brien et
706 al., 1995), and with increased winter precipitation in western Norway (Bjune et al.,
707 2005). The precipitation maxima throughout the middle Holocene may be explained by
708 the large scale atmospheric shifts associated with declining summer insolation during
709 this period (Knudsen et al., 2011). Specifically, the declining summer insolation gradient
710 between the high and low latitudes (Laskar et al., 2004), caused a southward
711 displacement of the ITCZ (Haug et al., 2001), the westerly jet across the North Atlantic
712 and the mean position of the Icelandic low (Harrison et al., 1992). Our new precipitation
713 data corroborates the scenario of Knudsen et al. (2011) that indicates that Iceland was
714 situated directly in the path of the southwardly displaced, moisture carrying westerlies
715 throughout the middle Holocene, and experienced high precipitation (Figs. 6c,d,e).

716 A clear correlation between increased precipitation in Iceland and NAO+ periods,
717 has been observed in the instrumental record (Hanna et al., 2004; Hurrell, 1995). Proxy
718 reconstructions of NAO variability now extend back through the MCA (Trouet et al.,
719 2009), to 5.2 kyrs BP (Olsen et al., 2012). If the contemporary link between increased
720 precipitation and NAO+ periods holds true throughout the Holocene, then our
721 precipitation records suggest that a persistent NAO+ atmospheric pattern was prevalent

722 from at least 7.5 kyrs BP onwards, lasting until the end of the middle Holocene at 3.2
723 kyr BP. Evidence for increased storminess during the middle Holocene in Iceland
724 (Jackson et al., 2005), along with a predominantly positive mode of the NAO, as
725 reconstructed from Greenland lake redox states for much of the middle Holocene
726 (Olsen et al., 2012) supports our hypothesis. Finally, the NAO may also have influenced
727 North Atlantic SSTs during the middle Holocene (Andersen et al., 2004), however such
728 variability is not obviously expressed in our $U^{K'}_{37}$-SST record.

729 **4.3. Late Holocene climate variability and the evolution of the modern NAO (3.2 -**
730 **0.3 ka)**

731 The late Holocene is the most socially relevant period in this study because of the
732 clear and persistent influence climatic fluctuations had on human societies (Buntgen et
733 al., 2011; D'Andrea et al., 2011; deMenocal, 2001). Our proxy records indicate that all
734 climate parameters, precipitation, air-, and sea surface temperature underwent
735 noteworthy change at the transition from the middle to the late Holocene (Figs. 6 and
736 7a, b, c, d, e).

737 From ~3.2 kyrs BP, the reconstructed CBT/MBT'-MAT and $U^{K'}_{37}$-SST temperature
738 trends deviate from the continually decreasing summer insolation (Figs 6a, b).
739 Intriguingly, the late Holocene is the only period where the CBT/MBT'-MAT
740 reconstruction does not follow insolation change. The simultaneous decoupling of both
741 CBT/MBT'-MAT and $U^{K'}_{37}$-SST records from insolation indicates a threshold, after
742 which, a driving mechanism other than insolation started to dominate air and sea
743 surface temperature variations over the most recent ~3.2 kyrs BP. Along with the
744 temperature records, the soil pH precipitation record indicates a gradual, while the
745 $ACL_{25\text{-}35}$ and dD_{C29} records show a more abrupt precipitation decrease (Figs 6 and 7c,
746 d, e). The periods from ~2.2 to ~1.3 kyrs BP, and from ~1.1 to ~0.5 kyrs BP are

747 characterised by relatively warm $U^{K'}_{37}$-SSTs, while CBT/MBT'-MATs tend to be cool,
748 and precipitation tends to be elevated. Within ^{14}C-AMS dating errors, these periods
749 coincide with the Roman Warm Period (RWP), and the MCA (Geirsdóttir et al., 2013;
750 Graham et al., 2011). In comparison, the periods from ~1.3 to ~1.1 kyrs BP, and from
751 ~0.5 kyrs BP to ~0.3 kyrs BP, are characterised by cooler $U^{K'}_{37}$-SSTs, warmer
752 CBT/MBT'MATs, and lower precipitation. These periods coincide with the Dark Ages
753 (DA; also known as the migration period; Buntgen et al., 2011; Sicre et al., 2008a) and
754 the onset of the LIA (Ogilvie and Jonsson, 2001). In contrast with the asynchronous
755 trends of precipitation, marine and terrestrial temperatures during the middle and early
756 Holocene, all climate proxy records exhibit changes over four distinct climatic periods
757 covering most of the late Holocene. This suggests one dominant controlling mechanism,
758 most plausibly the NAO, which is known to affect sea surface temperature, air
759 temperature and precipitation in Northern Europe and the North Atlantic sector (Hurrell,
760 1995; Hurrell et al., 2003). Assuming that the relationship between contemporary
761 instrumental observations of precipitation, sea surface-, and air temperatures, and the
762 NAO have remained constant throughout the late Holocene we would expect to observe
763 the following climatic variations during positive NAO phases (compared to negative
764 NAO phases): higher precipitation over Iceland (Hurrell, 1995; Hurrell et al., 2003; Figs.
765 1c, d), a higher throughput of warm Atlantic waters through the Denmark Strait, and
766 therefore warmer SSTs (Blindheim and Malmberg, 2005; Figs. 1e, f). Higher air
767 temperatures might also be expected, however, the link between air temperature and
768 NAO is tenuous on Iceland (Hanna et al., 2004; Ólafsdóttir et al., 2013). The variability
769 of the $U^{K'}_{37}$-SSTs and the precipitation records throughout the MCA and the LIA is in
770 good agreement with reconstructed NAO variability (Olsen et al., 2012; Trouet et al.,

771 2009; Figs. 6h, i and 7f, g), lending credence to our hypothesis that NAO was the
772 dominant forcing mechanism of Icelandic climate throughout the late Holocene.

773 Interestingly, Late Holocene centennial-scale CBT/MBT'-MAT variations are anti-
774 phased with $U^{K'}_{37}$-SST throughout the RWP, DA, MCA and LIA (Figs. 6 and 7a, b). This
775 would seemingly oppose contemporary (Hanna et al., 2004; Hurrell et al., 2003), and
776 proxy based observations (Ólafsdóttir et al., 2013), of warmer air temperatures during
777 NAO+ phases compared to NAO- phases. Specifically, the CBT/MBT'-MAT record
778 indicates relatively low temperatures during the RWP and MCA (NAO+), compared to
779 the higher reconstructed temperatures during the DA and LIA (NAO-). Additionally, the
780 reconstructed CBT/MBT'-MAT temperatures are higher than the chironomid based
781 August temperature reconstructed by Axford et al. (2009) during the DA and LIA, while
782 the temperature records are in better agreement during the RWP and MCA. This
783 suggests, that Icelandic CBT/MBT'-MAT temperature reconstructions provide
784 temperature estimates that are too high during the periods characterised by NAO-
785 periods. We hypothesise that this counterintuitive relationship between reconstructed
786 CBT/MBT'-MAT and NAO mode is due to the proxies molecular variations that are
787 mediated by soil bacteria, making the proxy a first order recorder of soil temperature
788 change (Weijers et al., 2007b). Contemporary observations show that negative
789 precipitation anomalies cause increased summer warmth throughout central Europe
790 and are correlated to NAO fluctuations due to decreased latent cooling from soil
791 moisture (Wang et al., 2011). Furthermore, dry soils warm more readily than wet soils
792 (Al-Kayssi et al., 1990). Thus we hypothesise that during NAO- periods (LIA, DA), while
793 precipitation was low (Fig. 6 and 7c, d, e), surface soils became relatively dry and were
794 warmed more easily by solar radiation, compared to the relatively wet soils of NAO+
795 periods (MCA, RWP). Consequently, the counterintuitive centennial scale CBT/MBT'-

796 MAT trends during the Late Holocene may indicate soil temperature variations as a
797 result of predominantly dry vs. predominantly wet soil conditions during the late
798 Holocene. Following this hypothesis, the CBT/MBT'-MAT proxy may indirectly provide
799 information on NAO variability via temperature dependency of the soil on changing
800 precipitation regimes. This is supported by the correlated CBT/MBT'-MAT and
801 precipitation records, demonstrating the advantage of considering multiple independent
802 biomarker records in concert.

803 The argument, that all proxy records shown here are mainly affected by NAO
804 fluctuations during the late Holocene, is supported by REDFIT spectral analyses
805 conducted on the $U^{K'}_{37}$-SST, CBT/MBT'-MAT, soil pH, and the ACL_{25-35}-proxy records
806 (Schulz and Mudelsee, 2002; Fig. 8). We note that the sampling resolution between
807 ~2.1 and ~7.3 kyrs BP is not high enough to resolve the high frequency periodicities
808 observed in the spectral analyses (SI 1). Therefore we limit the following interpretation
809 to the late Holocene, from ~2.1 to ~0.3 kyrs BP where the sample resolution is 25
810 years/sample. All four records reveal periodicities between 64 and 96 years at the 95%
811 significance level (Fig. 8). Such periodicities in instrumental records have been
812 associated with the NAO (Rossi et al., 2011). Moreover, these periodicities have also
813 been observed in the NAO reconstructions from Greenland lakes (Olsen et al., 2012),
814 and in a varve-thickness record from Iceland (Ólafsdóttir et al., 2013). We note that the
815 $U^{K'}_{37}$-SST and the CBT/MBT'-MAT temperature reconstructions also exhibit a significant
816 spectral peak at ~130 years which, along with the spectral peaks between 64 and 96
817 years is associated with the Atlantic Meridional Oscillation (AMO; Knudsen et al., 2011;
818 Rossi et al., 2011), that describes oscillatory variability of North Atlantic SSTs (Kerr,
819 2000; Schlesinger and Ramankutty, 1994). The influence of the AMO has also been
820 postulated in the varve-thickness record from Iceland (Ólafsdóttir et al., 2013).

821 Therefore it is plausible that the AMO, alongside the NAO played a role in the late
822 Holocene climate variations.

823 As discussed above, our biomarker proxies from MD99-2266 are likely weighted
824 towards a spring/summer signal, rather than mean annual climate variability. However,
825 the NAO is most prevalent during winter months (Hurrell, 1995; Hurrell and Deser,
826 2009). Thus we need to reconcile how biomarker proxies reconstructing summer
827 climate can detect an atmospheric signal that is most prevalent during winter months.
828 Hurrell and Deser (2009; and references therein) show that winter NAO indices can
829 affect the climate of the following year by affecting slower components of the climate
830 system (e.g. oceanic currents). Wang et al. (2011) show that European summer
831 temperatures are highly correlated with the NAO regime of the previous year.
832 Regionally, Blindheim and Malmberg (2005) have shown that changes of the winter sea
833 level pressure gradients across the Denmark Strait are significantly correlated with
834 SSTs of the following spring. Based on these observations in the instrumental record it
835 seems plausible that the biomarker records presented here are influenced by changing
836 NAO regimes, particularly when one considers that the sediment analysed for each data
837 point throughout the late Holocene integrates between 10 and 25 years of climate.

838 We suggest insolation ceased to be a dominant driver of centennial scale climate
839 events at the turn from the middle to the late Holocene. Instead, during this period of
840 relatively low insolation, the climatic influence of internal feedback mechanisms, namely
841 the NAO (and possibly the AMO) increasingly drove centennial scale changes, which
842 are superimposed on the longer term, monotonic, insolation driven change. This
843 suggests that lateral energy transport via warm surface currents and south-westerly
844 winds became more important for Icelandic climate, rather than continually decreasing

insolation. This conclusion is supported by a varve thickness record from lake Hvítárvatn which indicates, that the NAO exerted increasing influence on Icelandic climate throughout the late Holocene (Ólafsdóttir et al., 2013).

5. Conclusions

The high-resolution, multi-proxy approach to climate reconstruction that is presented in this study gives a comprehensive picture of terrestrial and marine climate evolution throughout the Holocene. We show that major reorganisations of Holocene climate in Iceland took place at two climatic thresholds, one at ~7.8, and the other at ~3.2 kyrs BP. Based on the apparent changing importance of different climate drivers at ~7.3 and ~3.2 kyrs BP, we divide the Holocene into three distinct climatic periods, the early, middle and late Holocene. These climatic threshold events only become evident when considering the high-resolution terrestrial and marine biomarker proxy data in concert, illustrating the importance of the multi-proxy approach adopted here.

The combination of multiple biomarker proxies increases overall confidence in our interpretations and also reveals strengths and weaknesses of a particular proxy. For example, the confidence we have in the interpretation of soil pH, $ACL_{25\text{-}35}$, and δD_{C29} as recorders of precipitation is increased by the fact that all three records are in good agreement. Furthermore, the multi-proxy approach also reveals that the CBT/MBT'-MAT record may be significantly influenced by precipitation along with air temperature. The counterintuitive behaviour of the CBT/MBT'-MAT record in the late Holocene can be explained if the precipitation proxies are considered.

CBT/MBT'-MATs were mainly driven by high insolation causing the terrestrial HTM throughout the early Holocene (10.7 - 7.8 kyrs BP). In contrast, $U^{K'}_{37}$-SSTs appear to be

868 dampened by the pervasive influence of glacial melt water events. Furthermore, the
869 centennial variability in the $U^{K'}_{37}$-SST record illustrates the influence of solar activity,
870 superimposed on the millennial scale melt water influence. The precipitation records
871 indicate a dryer than average early Holocene summer climate, driven by: a reduced
872 westerly jet during the summer months (Harrison et al., 1992) and reduced evaporation
873 in source waters, due to the pervasive influence of melt water events.

874 The influence of melt water on the $U^{K'}_{37}$-SST record ceases at the transition of the
875 early to the middle Holocene. Subsequently, an accelerating AMOC and decreasing, yet
876 still high insolation drove a strong marine HTM that occurred ~3 kyrs after its terrestrial
877 equivalent. The neoglacial period dominated the latter part of the middle Holocene and
878 was driven by continually decreasing insolation, although the decelerating AMOC likely
879 also affected $U^{K'}_{37}$-SSTs. Precipitation increased and remained high throughout the
880 middle Holocene. The transition from a dryer to wetter than average climate is attributed
881 to a decreasing summer insolation gradient that caused a southward shift of oceanic
882 (AMO) and atmospheric (Iceland low and westerlies jet) circulation systems (Harrison et
883 al., 1992; Knudsen et al., 2011). This shift placed Iceland under the direct influence of
884 moisture carrying westerlies and drove the high precipitation regime of the middle
885 Holocene.

886 All the paleoclimate records exhibit synchronous variability across four distinct
887 climatic periods, the RWP, DA, MCA and LIA in the late Holocene. The comparison
888 between of the precipitation, $U^{K'}_{37}$-SST and CBT/MBT'-MAT datasets presented here,
889 and the NAO reconstructions by Trouet et al. (2009) and Olsen et al. (2012) indicates
890 that the NAO became the dominant driver of Icelandic climate throughout the late
891 Holocene. Furthermore, In conjunction with the NAO reconstruction of Olsen et al.

892 (2012), our data demonstrates that the observed link between increased precipitation in
893 Iceland during NAO+ phases (Hurrell, 1995), that has previously been extended to the
894 beginning of the MCA (Trouet et al., 2009), may have existed nearly from the onset of
895 the middle Holocene at ~7.5 kyrs BP. Furthermore, assuming that NAO-type
896 atmospheric fluctuations are the primary driver of high precipitation throughout the
897 whole of the middle Holocene, our data indicates that the NAO was predominantly in a
898 positive mode from ~ 7.8 to ~3.2 kyrs BP. If the amount of precipitation can be
899 correlated with the strength of the westerlies ("strength" of the NAO), then our
900 precipitation data shows that the westerlies (and possibly the NAO) were considerably
901 stronger during the middle Holocene, compared to the late Holocene.

902 This study demonstrates that the interaction of different climate drivers drove the
903 complex Holocene climate history. It agrees with findings of Larsen et al. (2012) and
904 Geirsdóttir et al. (2013) who attribute the non-linear response of their palaeoclimate
905 reconstructions to insolation to regional and local climate feedback mechanisms. In light
906 of the fact that different climate drivers have shaped Icelandic climate throughout the
907 early, middle and late Holocene, trying to ascribe pervasive climatic cycles spanning the
908 entire Holocene (i.e. Bond cycles) to a single forcing mechanism would seemingly be
909 futile. This conclusion offers one explanation as to why so many researchers have not
910 been able to identify all, or even any Bond cycles in their Holocene records (Wanner et
911 al., 2011).

912 **6. <u>Acknowledgements</u>**

913 We thank an anonymous reviewer for the helpful and insightful comments. We
914 thank the crew and staff of the *Marion Dufresne II*, and the CALYPSO coring team on
915 the 1999 IMAGES cruise. We also thank Professor John Andrews for providing the core

916 material for this research, and the technical staff at the Institute of Arctic and Alpine
917 Research. We thank Dr. Richard Pancost and technical staff at the Organic
918 Geochemistry Unit, Bristol. We thank Dr. Ellen Roosen from the Woods Hole
919 Oceanographic Institution who sent additional u-channels of the top most 3.5 meters of
920 the sediment core archive half. We thank Dr. Fiona Meade for her help on Fig. 1
921 (https://sites.google.com/site/meadescientificservices). We thank the Scottish Alliance
922 for Geoscience, Environment and Society (SAGES) who funded the PhD to Dr. Heiko
923 Moossen. We thank the Japanese society for the promotion of science (JSPS) for
924 funding a two months bursary to Dr. Heiko Moossen to Hokkaido University.

925 **7. References**

926 Al-Kayssi, A.W., Al-Karaghouli, A.A., Hasson, A.M., Beker, S.A., 1990. Influence of Soil
927 Moisture Content on Soil Temperature and Heat Storage under Greenhouse Conditions.
928 Journal of Agricultural Engineering Research 45, 241-252.

929 Alley, R.B., Ágústsdóttir, A.M., 2005. The 8k event: cause and consequences of a major
930 Holocene abrupt climate change. Quaternary Science Reviews 24, 1123-1149.

931 Andersen, C., Koc, N., Jennings, A., Andrews, J.T., 2004. Nonuniform response of the
932 major surface currents in the Nordic Seas to insolation forcing: Implications for the
933 Holocene climate variability. Paleoceanography 19.

934 Andrews, J.T., Harðardóttir, J., Stoner, J.S., Principato, S.M., 2008. Holocene sediment
935 magnetic properties along a transect from Isafiardardiup to Djupall, Northwest Iceland.
936 Arctic Antarctic and Alpine Research 40, 1-14.

937 Andrews, J.T., Jennings, A.E., 2014. Multidecadal to millennial marine climate
938 oscillations across the Denmark Strait (similar to 66 degrees N) over the last 2000 cal yr
939 BP. Climate of the Past 10, 325-343.

940 Arnalds, O., 2008. Soils of Iceland. Jokull 58, 409-421.

941 Axford, Y., Andresen, C.S., Andrews, J.T., Belt, S.T., Geirsdóttir, Á., Massé, G., Miller,
942 G.H., Ólafsdóttir, S., Vare, L.L., 2011. Do paleoclimate proxies agree? A test comparing
943 19 late Holocene climate and sea-ice reconstructions from Icelandic marine and lake
944 sediments. Journal of Quaternary Science 26, 645-656.

945 Axford, Y., Geirsdóttir, Á., Miller, G., Langdon, P., 2009. Climate of the Little Ice Age and
946 the past 2000 years in northeast Iceland inferred from chironomids and other lake
947 sediment proxies. Journal of Paleolimnology 41, 7-24.

948 Badewien, T., Vogts, A., Dupont, L., Rullkötter, J., 2015. Influence of Late Pleistocene
949 and Holocene climate on vegetation distributions in southwest Africa elucidated from
950 sedimentary n-alkanes – Differences between 12°S and 20°S. Quaternary Science
951 Reviews 125, 160-171.

952 Bendle, J., Kawamura, K., Yamazaki, K., Niwai, T., 2007. Latitudinal distribution of
953 terrestrial lipid biomarkers and *n*-alkane compound-specific stable carbon isotope ratios
954 in the atmosphere over the western Pacific and Southern Ocean. Geochimica Et
955 Cosmochimica Acta 71, 5934-5955.

956 Bendle, J., Rosell-Melé, A., 2004. Distributions of U^{K}_{37} and $U^{K'}_{37}$ in the surface waters
957 and sediments of the Nordic Seas: Implications for paleoceanography. Geochemistry
958 Geophysics Geosystems 5.

959 Bendle, J.A.P., Rosell-Melé, A., 2007. High-resolution alkenone sea surface temperature
960 variability on the North Icelandic Shelf: implications for Nordic Seas palaeoclimatic
961 development during the Holocene. The Holocene 17, 9-24.

962 Bjune, A.E., Bakke, J., Nesje, A., Birks, H.J.B., 2005. Holocene mean July temperature
963 and winter precipitation in western Norway inferred from palynological and glaciological
964 lake-sediment proxies. The Holocene 15, 177-189.

965 Blindheim, J., Malmberg, S.-A., 2005. The Mean Sea Level Pressure Gradient Across the
966 Denmark Strait as an Indicator of Conditions in the North Icelandic Irminger Current, In:
967 Drange, H., Dokkken, T., Furevik, T., Gerdes, R., Berger, W. (Eds.), The Nordic Seas: An
968 Integrated Perspective. AGU, pp. 65-71.

969 Bond, G., Kromer, B., Beer, J., Muscheler, R., Evans, M.N., Showers, W., Hoffmann, S.,
970 Lotti-Bond, R., Hajdas, I., Bonani, G., 2001. Persistent solar influence on North Atlantic
971 climate during the Holocene. Science 294, 2130-2136.

972 Bond, G., Showers, W., Cheseby, M., Lotti, R., Almasi, P., deMenocal, P., Priore, P.,
973 Cullen, H., Hajdas, I., Bonani, G., 1997. A pervasive millennial-scale cycle in North
974 Atlantic Holocene and glacial climates. Science 278, 1257-1266.

975 Brassell, S.C., Eglinton, G., Marlowe, I.T., Pflaumann, U., Sarnthein, M., 1986. Molecular
976 Stratigraphy - A new tool for climatic assessment. Nature 320, 129-133.

977 Broecker, W.S., 1997. Thermohaline Circulation, the Achilles Heel of Our Climate
978 System: Will Man-Made CO2 Upset the Current Balance? Science 278, 1582-1588.

979 Buntgen, U., Tegel, W., Nicolussi, K., McCormick, M., Frank, D., Trouet, V., Kaplan, J.O.,
980 Herzig, F., Heussner, K.U., Wanner, H., Luterbacher, J., Esper, J., 2011. 2500 Years of
981 European Climate Variability and Human Susceptibility. Science 331, 578-582.

982 Calvo, E., Pelejero, C., Logan, G.A., De Deckker, P., 2004. Dust-induced changes in
983 phytoplankton composition in the Tasman Sea during the last four glacial cycles.
984 Paleoceanography 19, 10.

985 Caseldine, C., Geirsdottir, A., Langdon, P., 2003. Efstadalsvatn - a multi-proxy study of a
986 Holocene lacustrine sequence from NW Iceland. Journal of Paleolimnology 30, 55-73.

987 Castañeda, I.S., Schouten, S., 2011. A review of molecular organic proxies for examining
988 modern and ancient lacustrine environments. Quaternary Science Reviews 30, 2851-
989 2891.

990 Collins, J.A., Schefuß, E., Mulitza, S., Prange, M., Werner, M., Tharammal, T., Paul, A.,
991 Wefer, G., 2013. Estimating the hydrogen isotopic composition of past precipitation using
992 leaf-waxes from western Africa. Quaternary Science Reviews 65, 88-101.

993 Conte, M.H., Sicre, M.A., Rühlemann, C., Weber, J.C., Schulte, S., Schulz-Bull, D.,
994 Blanz, T., 2006. Global temperature calibration of the alkenone unsaturation index ($U^{K'37}$)
995 in surface waters and comparison with surface sediments. Geochemistry Geophysics
996 Geosystems 7.

997 Craig, H., 1961. Isotopic Variations in Meteoric Waters. Science 133, 1702-1703.

998 D'Andrea, W.J., Huang, Y., Fritz, S.C., Anderson, N.J., 2011. Abrupt Holocene climate
999 change as an important factor for human migration in West Greenland. Proceedings of
1000 the National Academy of Sciences of the United States of America 108, 9765-9769.

1001 deMenocal, P.B., 2001. Cultural responses to climate change during the Late Holocene.
1002 Science 292, 667-673.

1003 Eglinton, G., Gonzalez, A.G., Hamilton, R.J., Raphael, R.A., 1962. Hydrocarbon
1004 constituents of the wax coatings of plant leaves: a taxonomic survey. Phytochemistry 1,
1005 89 - 102.

1006 Eglinton, T.I., Eglinton, G., 2008. Molecular proxies for paleoclimatology. Earth and
1007 Planetary Science Letters 275, 1-16.

1008 Fawcett, P.J., Werne, J.P., Anderson, R.S., Heikoop, J.M., Brown, E.T., Berke, M.A.,
1009 Smith, S.J., Goff, F., Donohoo-Hurley, L., Cisneros-Dozal, L.M., Schouten, S., Sinninghe
1010 Damste, J.S., Huang, Y., Toney, J., Fessenden, J., WoldeGabriel, G., Atudorei, V.,
1011 Geissman, J.W., Allen, C.D., 2011. Extended megadroughts in the southwestern United
1012 States during Pleistocene interglacials. Nature 470, 518-521.

1013 Fietz, S., Huguet, C., Bendle, J., Escala, M., Gallacher, C., Herfort, L., Jamieson, R.,
1014 Martinez-Garcia, A., McClymont, E.L., Peck, V.L., Prahl, F.G., Rossi, S., Rueda, G.,
1015 Sanson-Barrera, A., Rosell-Mele, A., 2012. Co-variation of crenarchaeol and branched
1016 GDGTs in globally-distributed marine and freshwater sedimentary archives. Global and
1017 Planetary Change 92-93, 275-285.

1018 Gao, L., Nie, J., Clemens, S., Liu, W., Sun, J., Zech, R., Huang, Y., 2012. The
1019 importance of solar insolation on the temperature variations for the past 110 kyr on the
1020 Chinese Loess Plateau. Palaeogeography, Palaeoclimatology, Palaeoecology 317–318,
1021 128-133.

1022 Geirsdottir, A., Andrews, J.T., Olafsdottir, S., Helgadottir, G., Hardardottir, J., 2002. A 36
1023 Ky record of iceberg rafting and sedimentation from north-west Iceland. Polar Research
1024 21, 291-298.

1025 Geirsdottir, A., Miller, G.H., Axford, Y., Olafsdottir, S., 2009a. Holocene and latest
1026 Pleistocene climate and glacier fluctuations in Iceland. Quaternary Science Reviews 28,
1027 2107-2118.

1028 Geirsdóttir, Á., Miller, G.H., Larsen, D.J., Ólafsdóttir, S., 2013. Abrupt Holocene climate
1029 transitions in the northern North Atlantic region recorded by synchronized lacustrine
1030 records in Iceland. Quaternary Science Reviews 70, 48-62.

1031 Geirsdottir, A., Miller, G.H., Thordarson, T., Olafsdottir, K.B., 2009b. A 2000 year record
1032 of climate variations reconstructed from Haukadalsvatn, West Iceland. Journal of
1033 Paleolimnology 41, 95-115.

1034 Giraudeau, J., Grelaud, M., Solignac, S., Andrews, J.T., Moros, M., Jansen, E., 2010.
1035 Millennial-scale variability in Atlantic water advection to the Nordic Seas derived from
1036 Holocene coccolith concentration records. Quaternary Science Reviews 29, 1276-1287.

1037 Graham, N.E., Ammann, C.M., Fleitmann, D., Cobb, K.M., Luterbacher, J., 2011. Support
1038 for global climate reorganization during the "Medieval Climate Anomaly". Clim Dyn 37,
1039 1217-1245.

1040 Gray, L.J., Beer, J., Geller, M., Haigh, J.D., Lockwood, M., Matthes, K., Cubasch, U.,
1041 Fleitmann, D., Harrison, G., Hood, L., Luterbacher, J., Meehl, G.A., Shindell, D., van
1042 Geel, B., White, W., 2010. Solar influences on climate. Rev. Geophys. 48, 53.

1043 Gronvold, K., Oskarsson, N., Johnsen, S.J., Clausen, H.B., Hammer, C.U., Bond, G.,
1044 Bard, E., 1995. Ash layers from iceland in the Greenland GRIP ice core correlated with
1045 oceanic and land sediments. Earth and Planetary Science Letters 135, 149-155.

1046 Grootes, P.M., Stuiver, M., 1997. Oxygen 18/16 variability in Greenland snow and ice
1047 with 10^{-3}-10^{-5} year time resolution. J. Geophys. Res. 102, 26455-26470.

1048 Hall, I.R., Bianchi, G.G., Evans, J.R., 2004. Centennial to millennial scale Holocene
1049 climate-deep water linkage in the North Atlantic. Quaternary Science Reviews 23, 1529-
1050 1536.

1051 Hallsdottir, M., 1995. On the pre-settlement history of Icelandic vegetation. Buvisindi 9,
1052 17-29.

1053 Hammer, Ø., Harper, D.A.T., Ryan, P.D., 2001. PAST: Paleontoogical Statistics software
1054 package for education and data analysis. Palaeontologia Electroniac 4(1):9 pp., 2.17c ed.

1055 Hanna, E., Jonsson, T., Box, J.E., 2004. An analysis of Icelandic climate since the
1056 nineteenth century. International Journal of Climatology 24, 1193-1210.

1057 Hanna, E., Jonsson, T., Olafsson, J., Valdimarsson, H., 2006. Icelandic coastal sea
1058 surface temperature records constructed: Putting the pulse on air-sea-climate
1059 interactions in the northern North Atlantic. Part I: Comparison with HadISST1 open-ocean
1060 surface temperatures and preliminary analysis of long-term patterns and anomalies of
1061 SSTs around Iceland. Journal of Climate 19, 5652-5666.

1062 Hansen, B., Østerhus, S., 2000. North Atlantic-Nordic Seas exchanges. Progress In
1063 Oceanography 45, 109-208.

1064 Harrison, S.P., Prentice, I.C., Bartlein, P.J., 1992. Influence of insolation and glaciation
1065 on atmospheric circulation in the North Atlantic sector: Implications of general circulation
1066 model experiments for the Late Quaternary climatology of Europe. Quaternary Science
1067 Reviews 11, 283-299.

1068 Haug, G.H., Hughen, K.A., Sigman, D.M., Peterson, L.C., Röhl, U., 2001. Southward
1069 Migration of the Intertropical Convergence Zone through the Holocene. Science 293,
1070 1304-1308.

1071 Hopmans, E.C., Weijers, J.W.H., Schefuss, E., Herfort, L., Damste, J.S.S., Schouten, S.,
1072 2004. A novel proxy for terrestrial organic matter in sediments based on branched and
1073 isoprenoid tetraether lipids. Earth and Planetary Science Letters 224, 107-116.

1074 Howe, J.A., Austin, W.E.N., Forwick, M., Paetzel, M., Harland, R., Cage, A.G., 2010.
1075 Fjord systems and archives: a review. Geological Society, London, Special Publications
1076 344, 5-15.

1077 Hurrell, J.W., 1995. Decadal trends in the North Atlantic Oscillation - Regional
1078 temperatures and precipitation. Science 269, 676-679.

1079 Hurrell, J.W., Deser, C., 2009. North Atlantic climate variability: The role of the North
1080 Atlantic Oscillation. Journal of Marine Systems 78, 28-41.

1081 Hurrell, J.W., Kushiner, Y., Ottersen, G., Visbeck, M., 2003. An overview of the North
1082 Atlantic Oscillation. American Geophysical Union, Washington, DC, ETATS-UNIS.

1083 Ineson, S., Scaife, A.A., Knight, J.R., Manners, J.C., Dunstone, N.J., Gray, L.J., Haigh,
1084 J.D., 2011. Solar forcing of winter climate variability in the Northern Hemisphere. Nature
1085 Geosci 4, 753-757.

1086 Jackson, M.G., Oskarsson, N., Trønnes, R.G., McManus, J.F., Oppo, D.W., Grönvold, K.,
1087 Hart, S.R., Sachs, J.P., 2005. Holocene loess deposition in Iceland: Evidence for
1088 millennial-scale atmosphere-ocean coupling in the North Atlantic. Geology 33, 509-512.

1089 Jennings, A., Andrews, J., Wilson, L., 2011. Holocene environmental evolution of the SE
1090 Greenland Shelf North and South of the Denmark Strait: Irminger and East Greenland
1091 current interactions. Quaternary Science Reviews 30, 980-998.

1092 Jennings, A.E., Knudsen, K.L., Hald, M., Hansen, C.V., Andrews, J.T., 2002. A mid-
1093 Holocene shift in Arctic sea-ice variability on the East Greenland Shelf. Holocene 12, 49-
1094 58.

1095 Johnson, D.W., Hanson, P.J., Todd, D.E., Susfalk, R.B., Trettin, C.F., 1998. Precipitation
1096 Change and Soil Leaching: Field Results and Simulations from Walker Branch
1097 Watershed, Tennessee. Water, Air, & Soil Pollution 105, 251-262.

1098 Justwan, A., Koç, N., Jennings, A.E., 2008. Evolution of the Irminger and East Icelandic
1099 Current systems through the Holocene, revealed by diatom-based sea surface
1100 temperature reconstructions. Quaternary Science Reviews 27, 1571-1582.

1101 Kaufman, D.S., Ager, T.A., Anderson, N.J., Anderson, P.M., Andrews, J.T., Bartlein, P.J.,
1102 Brubaker, L.B., Coats, L.L., Cwynar, L.C., Duvall, M.L., Dyke, A.S., Edwards, M.E.,
1103 Eisner, W.R., Gajewski, K., Geirsdóttir, A., Hu, F.S., Jennings, A.E., Kaplan, M.R.,
1104 Kerwin, M.W., Lozhkin, A.V., MacDonald, G.M., Miller, G.H., Mock, C.J., Oswald, W.W.,
1105 Otto-Bliesner, B.L., Porinchu, D.F., Rühland, K., Smol, J.P., Steig, E.J., Wolfe, B.B.,
1106 2004. Holocene thermal maximum in the western Arctic (0-180°W). Quaternary Science
1107 Reviews 23, 529-560.

1108 Kawamura, K., Ishimura, Y., Yamazaki, K., 2003. Four years' observations of terrestrial
1109 lipid class compounds in marine aerosols from the western North Pacific. Global
1110 Biogeochem. Cycles 17, 1003.

1111 Kerr, R.A., 2000. A North Atlantic climate pacemaker for the centuries. Science 288,
1112 1984-1986.

1113 Knudsen, M.F., Seidenkrantz, M.-S., Jacobsen, B.H., Kuijpers, A., 2011. Tracking the
1114 Atlantic Multidecadal Oscillation through the last 8,000 years. Nature Communications 2.

1115 Langdon, P.G., Leng, M.J., Holmes, N., Caseldine, C.J., 2010. Lacustrine evidence of
1116 early-Holocene environmental change in northern Iceland: a multiproxy palaeoecology
1117 and stable isotope study. Holocene 20, 205-214.

1118 Larsen, D.J., Miller, G.H., Geirsdóttir, Á., Ólafsdóttir, S., 2012. Non-linear Holocene
1119 climate evolution in the North Atlantic: a high-resolution, multi-proxy record of glacier
1120 activity and environmental change from Hvítárvatn, central Iceland. Quaternary Science
1121 Reviews 39, 14-25.

1122 Laskar, J., Robutel, P., Joutel, F., Gastineau, M., Correia, A.C.M., Levrard, B., 2004. A
1123 long-term numerical solution for the insolation quantities of the Earth. Astronomy &
1124 Astrophysics 428, 261-285.

1125 LeGrande, A.N., Schmidt, G.A., 2008. Ensemble, water isotope-enabled, coupled general
1126 circulation modeling insights into the 8.2 ka event. Paleoceanography 23.

1127 Mayewski, P.A., Rohling, E.E., Stager, J.C., Karlen, W., Maasch, K.A., Meeker, L.D.,
1128 Meyerson, E.A., Gasse, F., van Kreveld, S., Holmgren, K., Lee-Thorp, J., Rosqvist, G.,
1129 Rack, F., Staubwasser, M., Schneider, R.R., Steig, E.J., 2004. Holocene climate
1130 variability. Quaternary Research 62, 243-255.

1131 Moossen, H., Abell, R., Quillmann, U., Bendle, J., 2013. Holocene changes in marine
1132 productivity and terrestrial organic carbon inputs into an Icelandic fjord: Application of
1133 molecular and bulk organic proxies. The Holocene 23, 11.

1134 Moros, M., Andrews, J.T., Eberl, D.D., Jansen, E., 2006. Holocene history of drift ice in
1135 the northern North Atlantic: Evidence for different spatial and temporal modes.
1136 Paleoceanography 21, PA2017.

1137 Niedermeyer, E.M., Schefuß, E., Sessions, A.L., Mulitza, S., Mollenhauer, G., Schulz, M.,
1138 Wefer, G., 2010. Orbital- and millennial-scale changes in the hydrologic cycle and
1139 vegetation in the western African Sahel: insights from individual plant wax δD and $\delta^{13}C$.
1140 Quaternary Science Reviews 29, 2996-3005.

1141 O'Brien, S.R., Mayewski, P.A., Meeker, L.D., Meese, D.A., Twickler, M.S., Whitlow, S.I.,
1142 1995. Complexity of Holocene climate as reconstructed from a Greendland ice core.
1143 Science 270, 1962-1964.

1144 Ogilvie, A.E.J., Jonsson, T., 2001. "Little Ice Age" research: A perspective from Iceland.
1145 Climatic Change 48, 9-52.

1146 Ólafsdóttir, K.B., Geirsdóttir, Á., Miller, G.H., Larsen, D.J., 2013. Evolution of NAO and
1147 AMO strength and cyclicity derived from a 3-ka varve-thickness record from Iceland.
1148 Quaternary Science Reviews 69, 142-154.

1149 Ólafsdóttir, S., Jennings, A.E., Geirsdóttir, Á., Andrews, J., Miller, G.H., 2010. Holocene
1150 variability of the North Atlantic Irminger current on the south- and northwest shelf of
1151 Iceland. Marine Micropaleontology 77, 101-118.

1152 Olsen, J., Anderson, N.J., Knudsen, M.F., 2012. Variability of the North Atlantic
1153 Oscillation over the past 5,200 years. Nature Geoscience 5, 808-812.

1154 Peterse, F., Kim, J.-H., Schouten, S., Kristensen, D.K., Koç, N., Sinninghe Damsté, J.S.,
1155 2009. Constraints on the application of the MBT/CBT palaeothermometer at high latitude
1156 environments (Svalbard, Norway). Organic Geochemistry 40, 692-699.

1157 Peterse, F., Nicol, G.W., Schouten, S., Sinninghe Damsté, J.S., 2010. Influence of soil
1158 pH on the abundance and distribution of core and intact polar lipid-derived branched
1159 GDGTs in soil. Organic Geochemistry 41, 1171-1175.

1160 Peterse, F., van der Meer, J., Schouten, S., Weijers, J.W.H., Fierer, N., Jackson, R.B.,
1161 Kim, J.-H., Sinninghe Damsté, J.S., 2012. Revised calibration of the MBT–CBT

paleotemperature proxy based on branched tetraether membrane lipids in surface soils. Geochimica et Cosmochimica Acta 96, 215-229.

Prahl, F.G., Rontani, J.F., Zabeti, N., Walinsky, S.E., Sparrow, M.A., 2010. Systematic pattern in $U^{K'37}$ Temperature residuals for surface sediments from high latitude and other oceanographic settings. Geochimica Et Cosmochimica Acta 74, 131-143.

Prahl, F.G., Wakeham, S.G., 1987. Calibration of unsaturation patterns in long-chain ketone compositions for paleotemperature assessment. Nature 330, 367-369.

Quillmann, U., Jennings, A., Andrews, J., 2010. Reconstructing Holocene palaeoclimate and palaeoceanography in Isafjaroardjup, northwest Iceland, from two fjord records overprinted by relative sea-level and local hydrographic changes. Journal of Quaternary Science 25, 1144-1159.

Quillmann, U., Marchitto, T.M., Jennings, A.E., Andrews, J.T., Friestad, B.F., 2012. Cooling and freshening at 8.2 ka on the NW Iceland Shelf recorded in paired $\delta^{18}O$ and Mg/Ca measurements of the benthic foraminifer *Cibicides lobatulus*. Quaternary Research 78, 528-539.

Renssen, H., Goosse, H., Fichefet, T., Brovkin, V., Driesschaert, E., Wolk, F., 2005. Simulating the Holocene climate evolution at northern high latitudes using a coupled atmosphere-sea ice-ocean-vegetation model. Clim Dyn 24, 23-43.

Rohling, E.J., Palike, H., 2005. Centennial-scale climate cooling with a sudden cold event around 8,200 years ago. Nature 434, 975-979.

Rommerskirchen, F., Eglinton, G., Dupont, L., Rullkötter, J., 2006a. Glacial/interglacial changes in southern Africa: Compound-specific δ13C land plant biomarker and pollen records from southeast Atlantic continental margin sediments. Geochemistry, Geophysics, Geosystems 7, Q08010.

Rommerskirchen, F., Plader, A., Eglinton, G., Chikaraishi, Y., Rullkötter, J., 2006b. Chemotaxonomic significance of distribution and stable carbon isotopic composition of long-chain alkanes and alkan-1-ols in C4 grass waxes. Organic Geochemistry 37, 1303-1332.

1190 Rossi, A., Massei, N., Laignel, B., 2011. A synthesis of the time-scale variability of
1191 commonly used climate indices using continuous wavelet transform. Global and
1192 Planetary Change 78, 1-13.

1193 Rueda, G., Fietz, S., Rosell-Mele, A., 2013. Coupling of air and sea surface temperatures
1194 in the eastern Fram Strait during the last 2000 years. Holocene 23, 692-698.

1195 Rueda, G., Rosell-Melé, A., Escala, M., Gyllencreutz, R., Backman, J., 2009. Comparison
1196 of instrumental and GDGT-based estimates of sea surface and air temperatures from the
1197 Skagerrak. Organic Geochemistry 40, 287-291.

1198 Sachse, D., Billault, I., Bowen, G.J., Chikaraishi, Y., Dawson, T.E., Feakins, S.J.,
1199 Freeman, K.H., Magill, C.R., McInerney, F.A., van der Meer, M.T.J., Polissar, P., Robins,
1200 R.J., Sachs, J.P., Schmidt, H.-L., Sessions, A.L., White, J.W.C., West, J.B., Kahmen, A.,
1201 2012. Molecular Paleohydrology: Interpreting the Hydrogen-Isotopic Composition of Lipid
1202 Biomarkers from Photosynthesizing Organisms. Annual Review of Earth and Planetary
1203 Sciences 40, 221-249.

1204 Schefuss, E., Ratmeyer, V., Stuut, J.-B.W., Jansen, J.H.F., Sinninghe Damsté, J.S.,
1205 2003. Carbon isotope analyses of n-alkanes in dust from the lower atmosphere over the
1206 central eastern Atlantic. Geochimica Et Cosmochimica Acta 67, 1757-1767.

1207 Schefuss, E., Schouten, S., Schneider, R.R., 2005. Climatic controls on central African
1208 hydrology during the past 20,000 years. Nature 437, 1003-1006.

1209 Schlesinger, M.E., Ramankutty, N., 1994. An oscillation in the global climate system of
1210 period 65-70 years. Nature 367, 723-726.

1211 Schlitzer, R., 2010. Ocean Data View, http://odv.awi.de.

1212 Schulz, M., Mudelsee, M., 2002. REDFIT: estimating red-noise spectra directly from
1213 unevenly spaced paleoclimatic time series. Computers & Geosciences 28, 421-426.

1214 Shanahan, T.M., Hughen, K.A., Van Mooy, B.A.S., 2013. Temperature sensitivity of
1215 branched and isoprenoid GDGTs in Arctic lakes. Organic Geochemistry 64, 119-128.

1216 Shindell, D.T., Schmidt, G.A., Mann, M.E., Rind, D., Waple, A., 2001. Solar Forcing of
1217 Regional Climate Change During the Maunder Minimum. Science 294, 2149-2152.

1218 Sicre, M.A., Hall, I.R., Mignot, J., Khodri, M., Ezat, U., Truong, M.X., Eiríksson, J.,
1219 Knudsen, K.L., 2011. Sea surface temperature variability in the subpolar Atlantic over the
1220 last two millennia. Paleoceanography 26, PA4218.

1221 Sicre, M.A., Jacob, J., Ezat, U., Rousse, S., Kissel, C., Yiou, P., Eiriksson, J., Knudsen,
1222 K.L., Jansen, E., Turon, J.L., 2008a. Decadal variability of sea surface temperatures off
1223 North Iceland over the last 2000 years. Earth and Planetary Science Letters 268, 137-
1224 142.

1225 Sicre, M.A., Yiou, P., Eiriksson, J., Ezat, U., Guimbaut, E., Dahhaoui, I., Knudsen, K.L.,
1226 Jansen, E., Turon, J.L., 2008b. A 4500-year reconstruction of sea surface temperature
1227 variability at decadal time-scales off North Iceland. Quaternary Science Reviews 27,
1228 2041-2047.

1229 Siddall, M., Abe-Ouchi, A., Andersen, M., Antonioli, F., Bamber, J., Bard, E., Clark, J.,
1230 Clark, P., Deschamps, P., Dutton, A., Elliot, M., Gallup, C., Gomez, N., Gregory, J.,
1231 Huybers, P., Kawarnura, K., Kelly, M., Lambeck, K., Lowell, T., Milrovica, J., Otto-
1232 Bliesner, B., Richards, D., Stanford, J., Stirling, C., Stocker, T., Thomas, A., Thompson,
1233 B., Toernqvist, T., Vazquez Riveiros, N., Waelbroeck, C., Yokoyama, Y., Yu, S., Grp,
1234 P.L.W., 2010. The sea-level conundrum: case studies from palaeo-archives. Journal of
1235 Quaternary Science 25, 19-25.

1236 Sikes, E.L., Volkman, J.K., Robertson, L.G., Pichon, J.-J., 1997. Alkenones and alkenes
1237 in surface waters and sediments of the Southern Ocean: Implications for
1238 paleotemperature estimation in polar regions. Geochimica Et Cosmochimica Acta 61,
1239 1495-1505.

1240 Sinninghe Damsté, J.S., Rijpstra, W.I.C., Hopmans, E.C., Weijers, J.W.H., Foesel, B.U.,
1241 Overmann, J., Dedysh, S.N., 2011. 13,16-Dimethyl Octacosanedioic Acid (iso-Diabolic
1242 Acid), a Common Membrane-Spanning Lipid of Acidobacteria Subdivisions 1 and 3.
1243 Applied and Environmental Microbiology 77, 4147-4154.

1244 Smittenberg, R.H., Eglinton, T.I., Schouten, S., Sinninghe Damsté, J.S., 2006. Ongoing
1245 Buildup of Refractory Organic Carbon in Boreal Soils During the Holocene. Science 314,
1246 1283-1286.

1247 Solanki, S.K., Usoskin, I.G., Kromer, B., Schussler, M., Beer, J., 2004. Unusual activity of
1248 the Sun during recent decades compared to the previous 11,000 years. Nature 431,
1249 1084-1087.

1250 Ternois, Y., Sicre, M.A., Boireau, A., Beaufort, L., Miquel, J.C., Jeandel, C., 1998.
1251 Hydrocarbons, sterols and alkenones in sinking particles in the Indian Ocean sector of
1252 the Southern Ocean. Organic Geochemistry 28, 489-501.

1253 Trouet, V., Esper, J., Graham, N.E., Baker, A., Scourse, J.D., Frank, D.C., 2009.
1254 Persistent Positive North Atlantic Oscillation Mode Dominated the Medieval Climate
1255 Anomaly. Science 324, 78-80.

1256 Vage, K., Pickart, R.S., Spall, M.A., Valdimarsson, H., Jonsson, S., Torres, D.J.,
1257 Osterhus, S., Eldevik, T., 2011. Significant role of the North Icelandic Jet in the formation
1258 of Denmark Strait overflow water. Nature Geoscience 4, 723-727.

1259 Vogts, A., Moossen, H., Rommerskirchen, F., Rullkotter, J., 2009. Distribution patterns
1260 and stable carbon isotopic composition of alkanes and alkan-1-ols from plant waxes of
1261 African rain forest and savanna C3 species. Organic Geochemistry 40, 1037-1054.

1262 Vogts, A., Schefuss, E., Badewien, T., Rullkötter, J., 2012. n-Alkane parameters from a
1263 deep sea sediment transect off southwest Africa reflect continental vegetation and
1264 climate conditions. Organic Geochemistry 47, 109-119.

1265 Waelbroeck, C., Labeyrie, L., Michel, E., Duplessy, J.C., McManus, J.F., Lambeck, K.,
1266 Balbon, E., Labracherie, M., 2002. Sea-level and deep water temperature changes
1267 derived from benthic foraminifera isotopic records. Quaternary Science Reviews 21, 295-
1268 305.

1269 Wang, G., Dolman, A.J., Alessandri, A., 2011. A summer climate regime over Europe
1270 modulated by the North Atlantic Oscillation. Hydrology and Earth System Sciences 15,
1271 57-64.

1272 Wanner, H., Solomina, O., Grosjean, M., Ritz, S.P., Jetel, M., 2011. Structure and origin
1273 of Holocene cold events. Quaternary Science Reviews 30, 3109-3123.

1274 Wastl, M., Stötter, J., Caseldine, C., 2001. Reconstruction of Holocene Variations of the
1275 Upper Limit of Tree or Shrub Birch Growth in Northern Iceland Based on Evidence from
1276 Vesturardalur-Skidadalur, Trölaskagi. Arctic, Antarctic, and Alpine Research 33, 191-203.

1277 Weijers, J.W.H., Bernhardt, B., Peterse, F., Werne, J.P., Dungait, J.A.J., Schouten, S.,
1278 Sinninghe Damsté, J.S., 2011. Absence of seasonal patterns in MBT-CBT indices in mid-
1279 latitude soils. Geochimica Et Cosmochimica Acta 75, 3179-3190.

1280 Weijers, J.W.H., Schefuss, E., Schouten, S., Sinninghe Damsté, J.S., 2007a. Coupled
1281 thermal and hydrological evolution of tropical Africa over the last deglaciation. Science
1282 315, 1701-1704.

1283 Weijers, J.W.H., Schouten, S., van den Donker, J.C., Hopmans, E.C., Sinninghe Damsté,
1284 J.S., 2007b. Environmental controls on bacterial tetraether membrane lipid distribution in
1285 soils. Geochimica Et Cosmochimica Acta 71, 703-713.

1286 Zhu, C., Weijers, J.W.H., Wagner, T., Pan, J.-M., Chen, J.-F., Pancost, R.D., 2011.
1287 Sources and distributions of tetraether lipids in surface sediments across a large river-
1288 dominated continental margin. Organic Geochemistry 42, 376-386.

1289

1290

1291

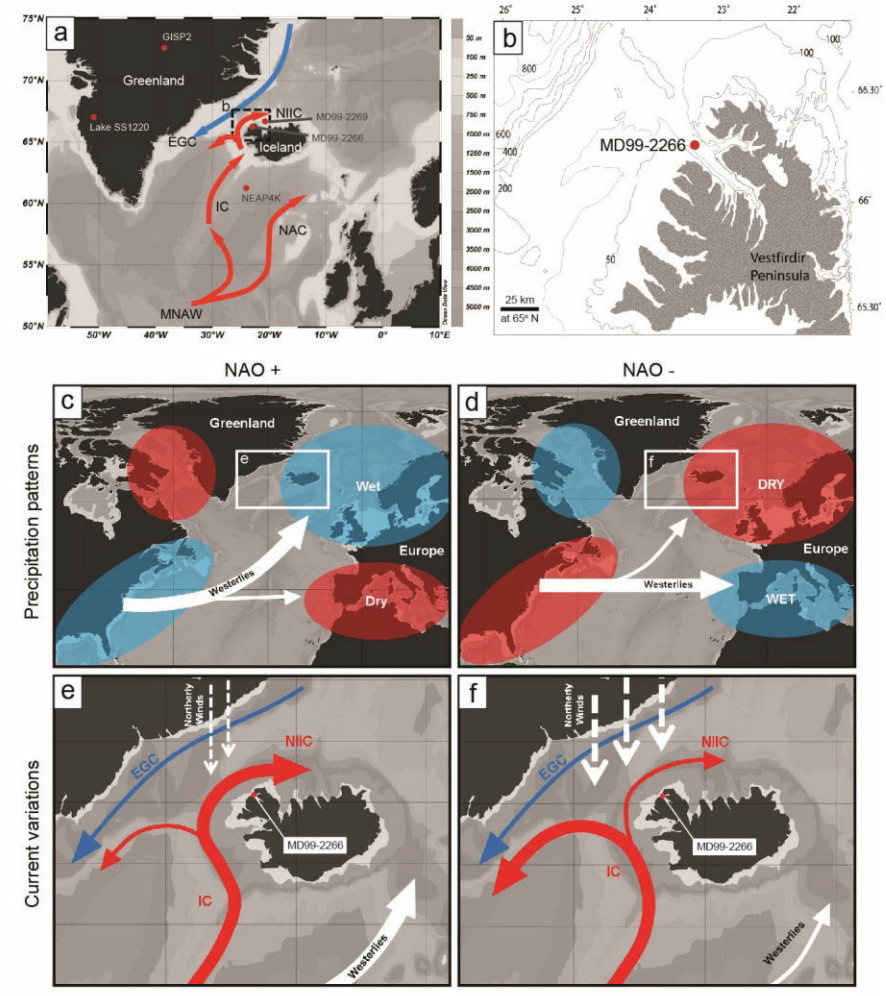

Figure 1: North Atlantic atmospheric and oceanic currents affecting the core (MD99-2266) location in the Denmark Strait. (a) Surface currents after Hansen and Østerhus (2000). Red arrows represent the Mean North Atlantic Water (MNAW) that branches into the North Atlantic Current (NAC) and the Irminger Current (IC). Part of the IC flows into the Denmark Strait and forms the North Icelandic Irminger Current (NIIC). The blue arrow represents the East Greenland Current (EGC). Core locations of compared datasets (Fig. 6), and of MD99-2266 are indicated by red dots. (b) Bathymetric map of Vestfirdir Peninsula with the core location (red dot) indicated in the mouth of Ísafjarðardjúp fjord. (c-f) Present day NAO influenced precipitation and current patterns. Iceland receives more precipitation during NAO+ (c), and less precipitation during NAO- (d) phases (Hurrell, 1995; precipitation patterns after: http://www.ldeo.columbia.edu/res/pi/NAO; Hurrell et al., 2003). NAO+ phases coincide with an increased Atlantic water influence on the North Icelandic Shelf and in the Denmark Strait, and decreased prevalence of northerly winds (e), and NAO- phases coincide with less Atlantic water influence in the Denmark Strait, and increased prevalence of northerly winds (f; Blindheim and Malmberg, 2005). Source of map:(Schlitzer, 2010).

1292

1293

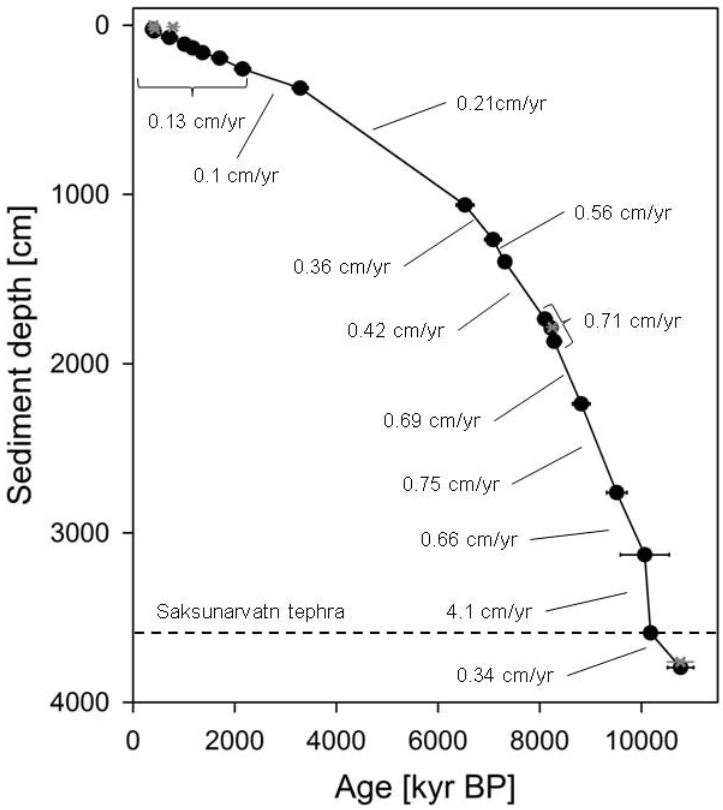

Figure 2: Age model of core MD99-2266 based on 19 (of a total of 24) ^{14}C-AMS dated sediment horizons and the depth horizon of the Saksunarvatn tephra (dashed line) which is dated at 10,180 ± 120 kyrs BP (Gronvold et al., 1995; Quillmann et al., 2010). The 5 ^{14}C-AMS dates discarded by Quillmann et al.(2010) are shown in grey. Sedimentation rates are calculated using the calibrated ages (kyr BP) of the dated horizons.

1294

1295

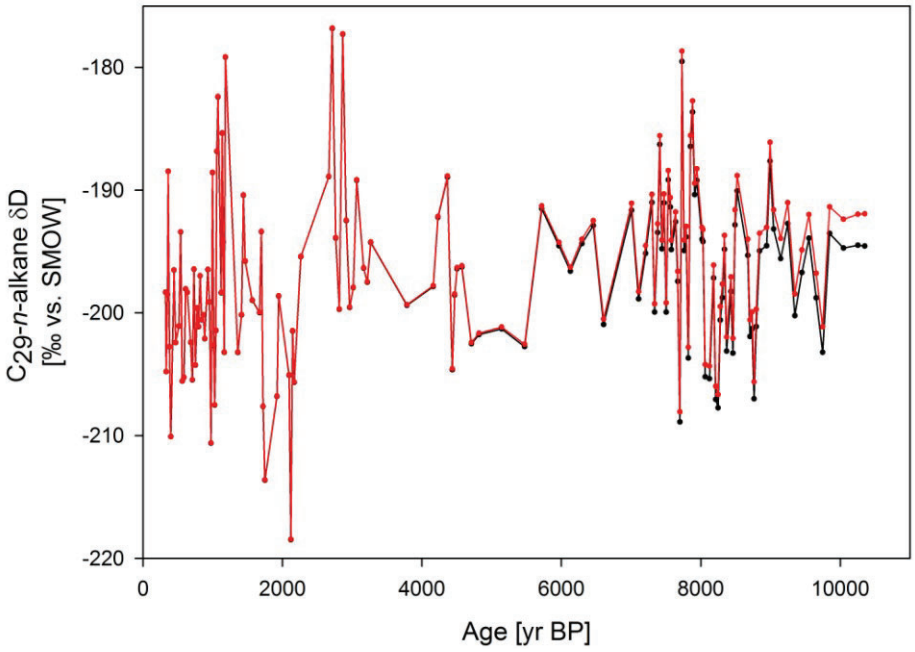

Figure 3: δD values of the C_{29}-*n*-alkane (black line and dots) and ice volume corrected δD values of the C_{29}-*n*-alkane (red line and dots).

1296

1297

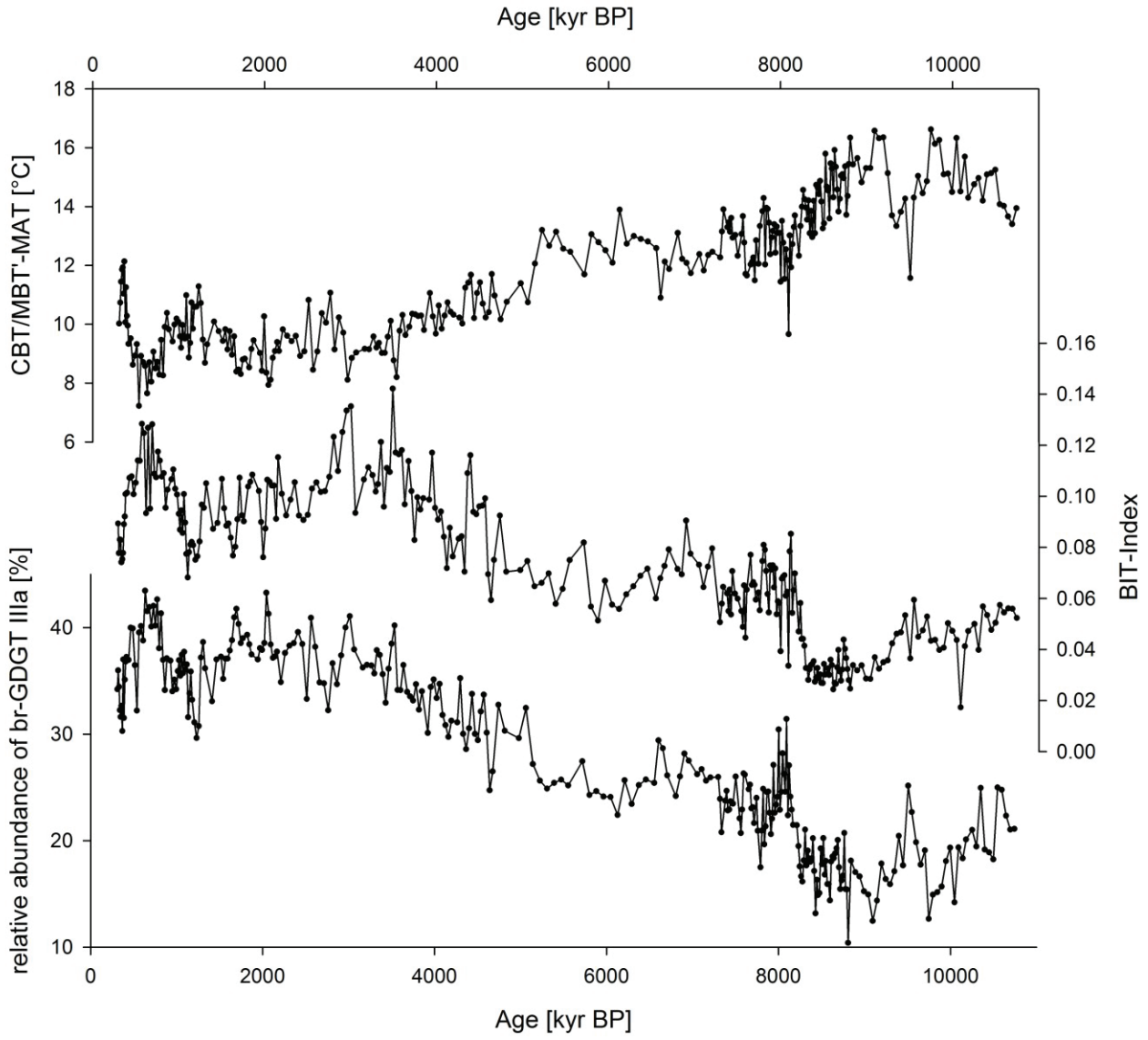

Figure 4: Temporal variability of the relative abundance of br-GDGT IIIa related to changes of the BIT-index (Moossen et al., 2013), and the CBT/MBT'-MAT reconstructions of Ísafjarðardjúp fjord.

1298

1299

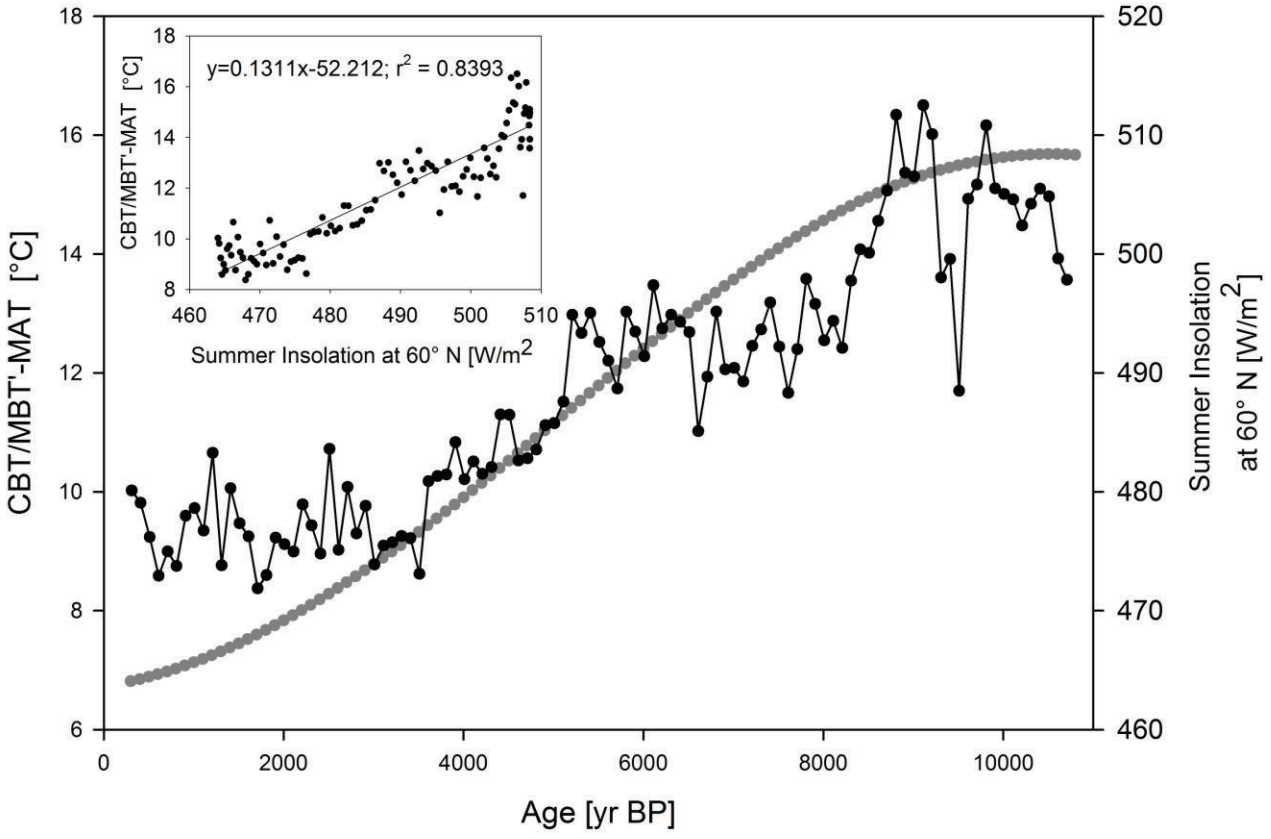

Figure 5: Regularly interpolated (sample interval = 100 years) CBT/MBT'-MATs (black dots and line) vs. summer insolation change (grey dots and line; sample interval = 100 years; Laskar et al., 2004). Inset: Linear correlation between CBT/MBT'-MAT and summer insolation.

1300

1301

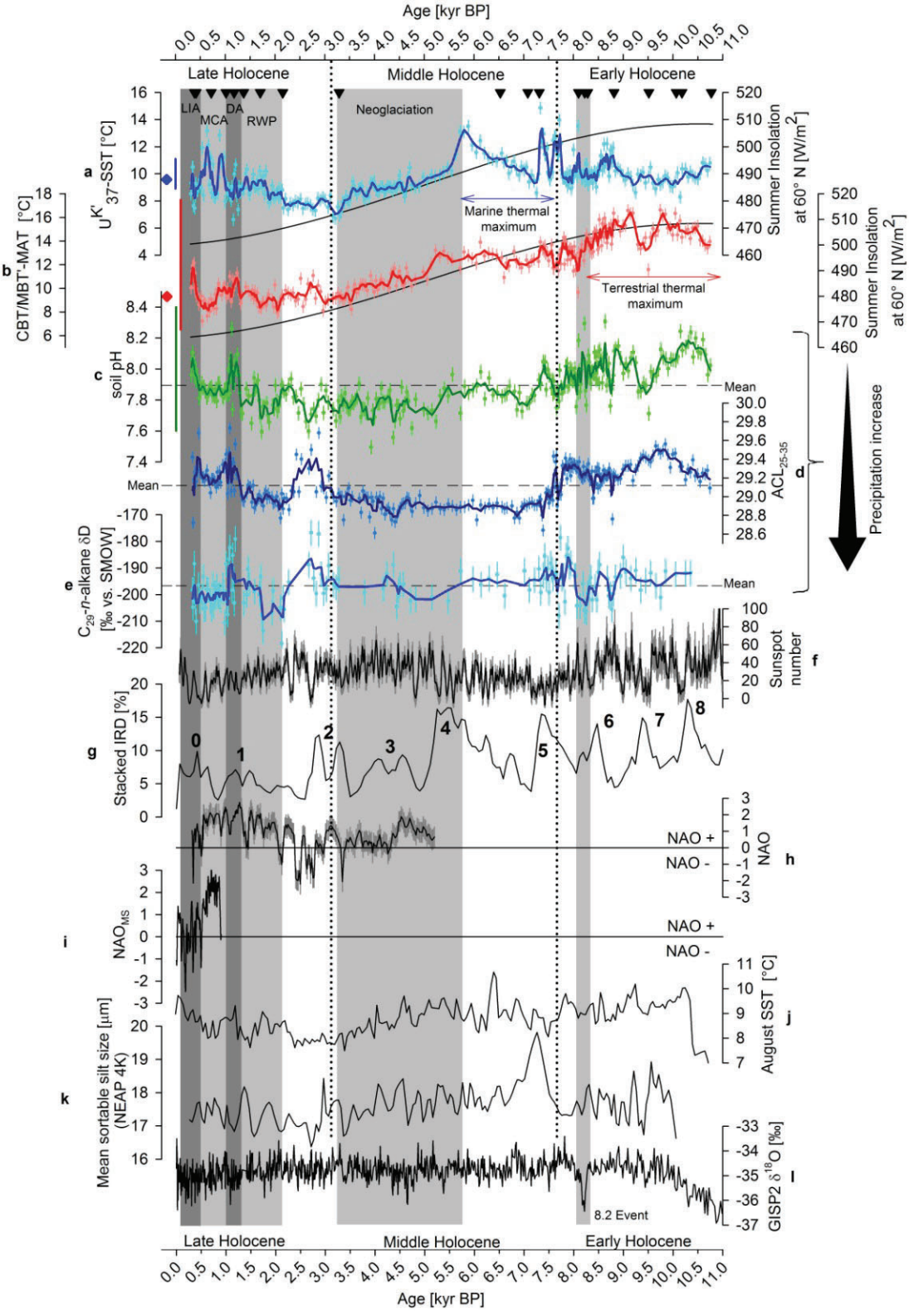

Figure 6: Iceland climate records compared with other North Atlantic paleoclimatic records. The LIA, MCA, DA (Dark Ages), RWP (Roman Warm Period), neoglaciation, and the 8.2 ka event are highlighted in shades of grey. The dotted horizontal lines indicate the division from early to middle, and from middle to late Holocene at 7.8 and 3.2 kyrs BP. **(a)** alkenone derived $U^{K'}_{37}$-SSTs. Raw data and 1σ SD (light blue) overlain by the 3-point moving average (dark blue), plotted against summer

insolation change (black line). The vertical blue bar indicates the uncertainty of the calibration equation (1.1 °C; Conte et al., 2006), the blue diamond indicates mean instrumental JJA SSTs at Stykkishólmur (Hanna et al., 2006). Black triangles indicate the ^{14}C-AMS dated horizons of MD99-2266. **(b)** br-GDGT derived CBT/MBT'-MAT. Raw data and 1σ SD (light red) overlaid by the 3-point moving (dark red) is plotted against summer insolation (black line). The vertical red bar indicates the uncertainty of the calibration equation (5.0 °C; Peterse et al., 2012). The red diamond indicates mean instrumental JJA air temperatures at Stykkishólmur (Hanna et al., 2004). **(c)** br-GDGT derived soil pH reconstruction. Raw data and 1σ SD (light green) overlain by the 3-point moving average (dark green). The vertical green bar indicates the uncertainty of the calibration equation (Root mean square error: 0.8; Peterse et al., 2012). **(d)** Average chain length variability of leaf wax derived *n*-alkanes ($ACL_{25\text{-}35}$) reconstructing precipitation variability. Raw data and 1σ SD (blue) overlain by the 3-point moving average (dark blue). **(e)** δD_{C29} reconstructing precipitation change. Raw data and 1σ SD (cyan) overlain by the 3-point moving average (blue). The dashed horizontal lines (c-e) indicate the mean Holocene precipitation as indicated by the respective records. **(f)** Holocene sunspot record (Solanki et al., 2004). **(g)** Stacked ice rafted debris (IRD) record revealing numbered Bond-cycles (Bond et al., 2001). **(h)** NAO variability after Olsen et al. (2012). **(i)** NAO variability after Trouet et al. (2009). **(j)** August SSTs on the North Icelandic Shelf after Justwan et al. (2008). **(k)** Mean sortable silt size of the Iceland-Scotland-Overflow-Waters (ISOW) south of Iceland after Hall et al. (2004). **(l)** GISP 2 δ^{18}O inferred temperature variations of the North Atlantic area after Grootes and Stuiver (1997).

1302

1303

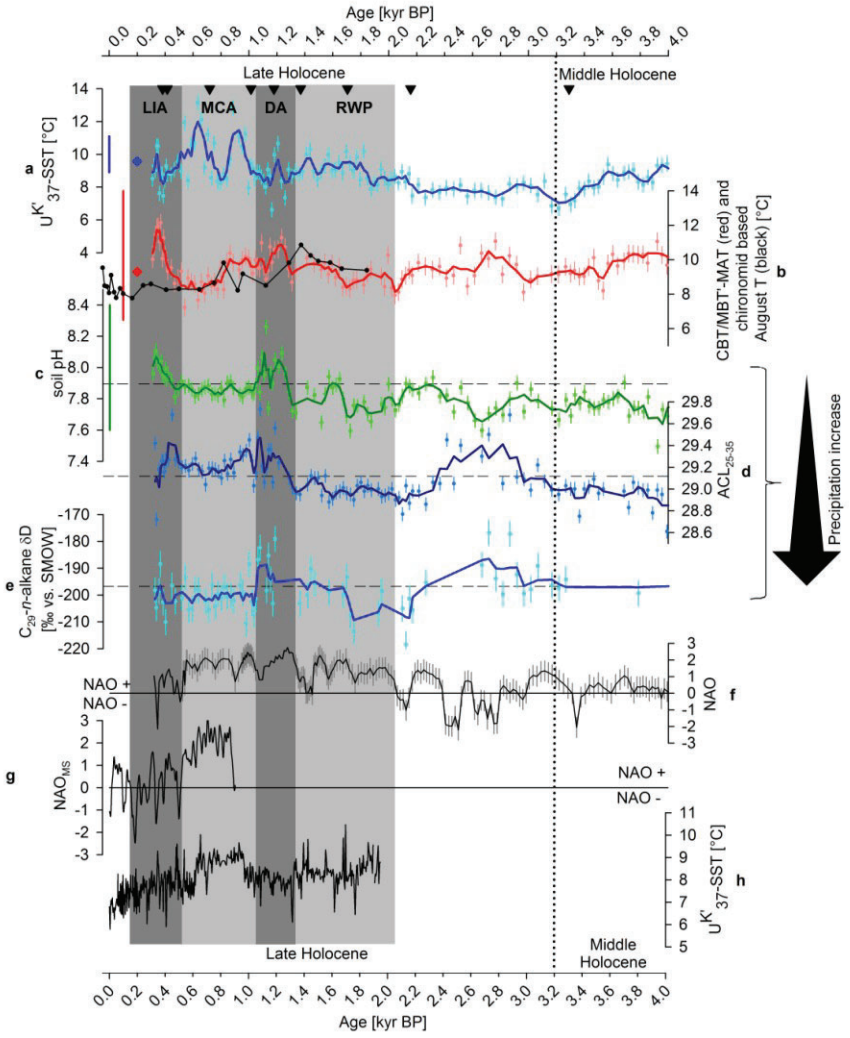

Figure 7: Iceland climate records of the youngest 4 kyrs BP. The LIA, the MCA, the DA, and the RWP are highlighted in shades of grey. The dotted horizontal line indicates the transition from the middle to the late Holocene. **(a)** $U^{K'}_{37}$-SST, raw data and analytical error (1σ SD) is shown in light blue overlain by the 3-point moving average in dark blue. The vertical blue bar indicates the uncertainty of the calibration equation (1.1 °C; Conte et al., 2006). The blue diamond indicates mean instrumental JJA SSTs at Stykkishólmur (Hanna et al., 2006). Black triangles indicate the ^{14}C-AMS dated horizons of MD99-2266. **(b)** CBT/MBT'-MAT raw data and analytical error (1σ SD) (light red) overlain by the 3-point moving average (dark red). The vertical red bar indicates the uncertainty of the calibration equation (5.0 °C; Peterse et al., 2012). The red diamond indicates mean instrumental JJA air temperatures at Stykkishólmur (Hanna et al., 2004). The black line and data points shows chironomide based August SSTs from north Iceland (Axford et al., 2009). **(c)** soil pH reconstruction raw data and analytical error (1σ SD; light green) overlain by 3-point moving average (dark green). The vertical green bar indicates the uncertainty of the calibration equation (0.8; Peterse et al., 2012). **(d)** Average chain length variability of leaf wax derived *n*-alkanes (ACL_{25-35}) raw data and analytical error (1σ SD; blue) overlain by the 3-point moving average (dark blue). **(e)** δD_{C29} raw data and analytical error (1σ SD; cyan) overlain by the 3-point moving average (blue). The dashed horizontal lines (c-e) indicate the mean Holocene precipitation as indicated by the respective records. **(f)** NAO variability after Olsen et al. (2012). **(g)** NAO variability after Trouet et al. (2009). **(h)** $U^{K'}_{37}$-SST reconstruction from the North Icelandic Shelf (Sicre et al., 2011).

1304

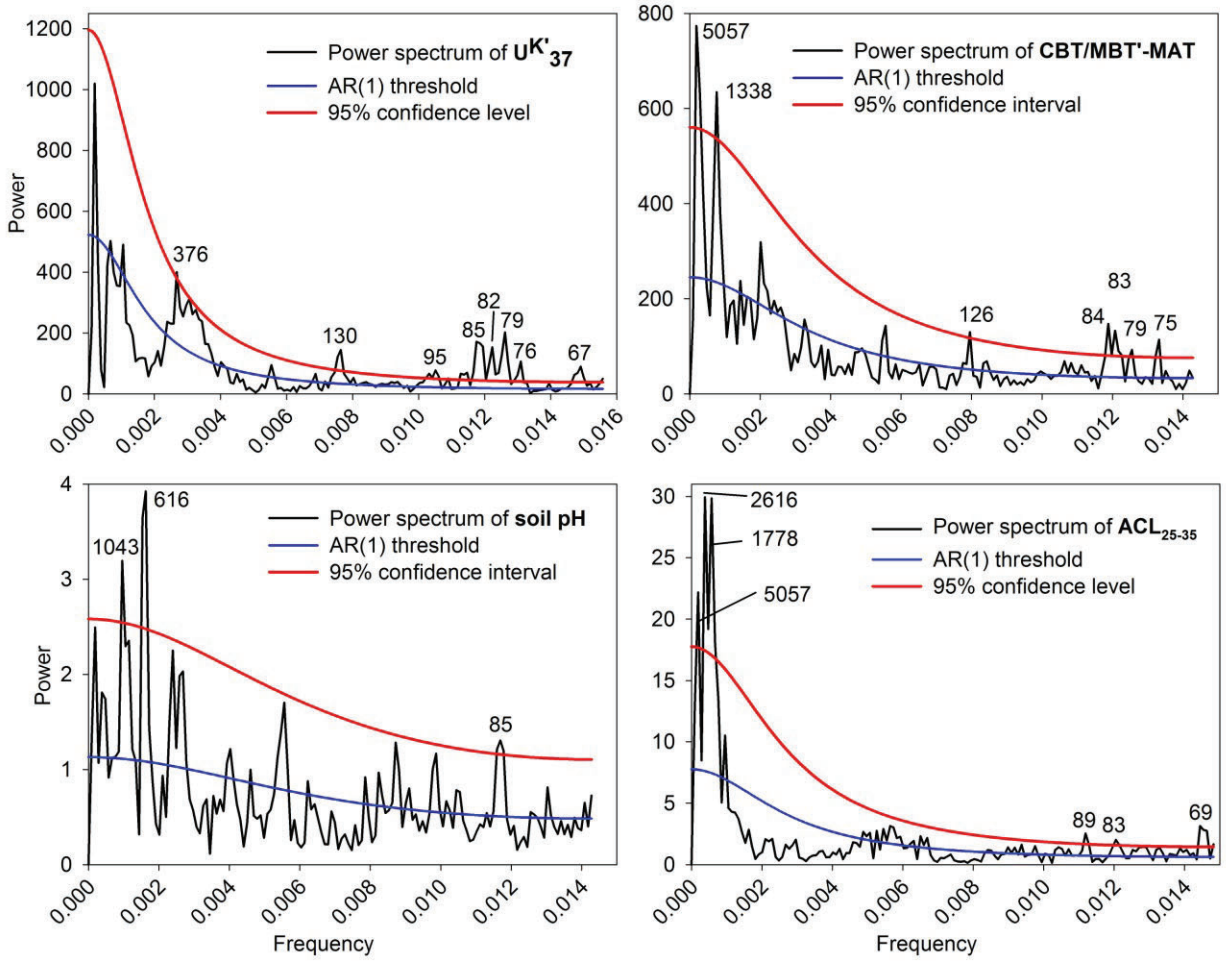

Figure 8: REDFIT power spectra of the $U^{K'}_{37}$-SST, CBT/MBT'-MAT, soil pH and ACL_{25-35} time series. The blue line delimits the AR(1) red noise model threshold. The red line indicates the 95 % confidence interval. The periodicities (years) of significant spectral peaks is indicated in each spectrum.

1305